Chapter 1

Scaling in Magnetic Materials

Krzysztof Z. Sokalski, Barbara Ślusarek and Jan Szczygłowski

Additional information is available at the end of the chapter

http://dx.doi.org/10.5772/63285

Abstract

The chapter presents applications of the scaling in several problems of magnetic materials. Soft magnetic materials (SMMs) and soft magnetic composites (SMCs) are considered. Application of scaling in investigations of problems, such as power losses, losses separation, data collapse of the losses characteristics and modelling of the magnetic hysteresis, is presented. The symmetry group generated by scaling and gauge transformations enables us to introduce the classification of the hysteresis loops with respect to the equivalence classes. SMC materials require special treatment in the production process. Therefore, algorithms for optimization of the power losses are created. The algorithm for optimization processes is based on the scaling and the notion of the pseudo-equation of state. The scaling makes modelling and calculations easy; however, the data must obey the scaling. Checking procedure of statistical data to this respect is presented.

Keywords: magnetic materials, hysteresis loop, power losses, losses separation, scaling, gauge

1. Introduction

The notion of scaling describes invariance of various phenomena and their mathematical models with respect to a change of scale. Let us take into account the simplest mathematical model revealing such behaviour:

$$y = Ax^{\alpha}. \tag{1}$$

where α and A are the constants of model. Such functions appear in mathematical modelling in physics, mathematics, biology, economics and engineering. In this section, we consider data of classical gas. By simple calculation, we will prove that these data are self-similar. Let us change the scale of the both variables x and y with respect to $\lambda > 0$ multiplier.

$$x' = \lambda^{\beta} x, y' = \lambda^{\gamma} y. \tag{2}$$

Substituting (2)–(1) we obtain:

$$y' = A' x'^{\alpha}, \tag{3}$$

where β and γ are scaling exponents and $A' = \lambda^{\gamma-\alpha\beta} A$ is the model constant in new scale. (1)–(3) reveal that the phenomenon described by the model (1) is self-similar. This means that the phenomenon reproduces itself on different scales. In achieving the property of self-similarity, an important role plays dimensional analysis. Its idea is very simple: physical laws cannot depend on an arbitrary choice of basic units of measurement [1]. Set of all transformations (2) and multiplication constitutes $\mathcal{G}_{\lambda}=(\mathbb{R}_{+}, \cdot)$ group. In the next section, we will consider self-similar model of hysteresis loop. Extension of (2) to the two parameters group is necessary to this respect. Let us extend (1) to non-homogenous form:

$$y = Ax^{\alpha} + \mathrm{c}, \tag{4}$$

The full symmetry of (4) consists of the two transformations, λ scaling and χ gauge transformation:

$$y' = A(\lambda x)^{\alpha} + c + \chi. \tag{5}$$

where χ is additive gauge operation which constitutes additive group $\mathcal{G}_{\chi}=(\mathbb{R}, +)$. Therefore, the full symmetry of (5) consists of the following direct product: $\mathcal{G}_{\lambda,\chi} = \mathcal{G}_{\lambda} \times \mathcal{G}_{\chi}$ [2]. However, the symmetry of the hysteresis loop will occur to be semi-direct product.

In this chapter, we will consider more advanced function and then the models (1) and (4). Therefore, we will need definition of homogenous function in general sense [3] which has played crucial role in the all achievements presented in this chapter. Let $f(x_1, x_2, \ldots x_n)$ be a function of n variables. If $\exists (\alpha_0, \alpha_1, \alpha_2, \ldots \alpha_n) \mathbb{R}^{n+1}$ such that $\forall \lambda \mathbb{R}_{+}$, the following relation holds:

$$\lambda^{\alpha_0} f\left(x_1, x_2, \ldots x_n\right) = f\left(\lambda^{\alpha_1} x_1, \lambda^{\alpha_2} x_2, \ldots \lambda^{\alpha_n} x_n\right). \tag{6}$$

Then, $f(x_1, x_2, \ldots x_n)$ is homogenous function in general sense. Based on the measurement data of classical gas presented in **Table 1**, we present simple application of this notion. We assume that the phenomena are represented by measurement data which satisfy certain relation called law. Let us assume that searched on phenomenon have a form of the homogenous function in general sense:

$$\lambda^a \rho(T,p) = \rho\left(\lambda^b T, \lambda^g p\right). \tag{7}$$

ρ[mol·m^{-3}]	T[K]	p[Pa]
0.096	500	400
0.090	515	385
0.084	530	370
0.078	545	355
0.073	560	340
0.068	575	325
0.063	590	310
0.059	605	295
0.054	620	280
0.050	635	265
0.046	650	250

Table 1. Measurement data of classical gas.

where ρ, T and p are gas density, temperature and pressure, respectively. Coefficients a, b and c are the scaling exponents. Since (7) holds for each value of λ, we are free to substitute the following expression $\lambda = T^{-1/b}$ and get the following relation:

$$T^{-a/b}\rho(T,p) = \rho\left(1, T^{-g/b}p\right). \tag{8}$$

Introducing new symbols for the scaling exponents: $\alpha = \frac{a}{b}$, $\gamma = \frac{g}{b}$ we derive the following equation of state:

$$T^{-\alpha}\rho = AT^{-\gamma}p. \tag{9}$$

where the right-hand side of (8) was approximated by linear function, A is an expansion's coefficient. In the next sections of this chapter, we will use the Maclaurin expansion beyond

the linear term as a way for creation of scaling function. Equation (9) depends on the one effective exponent $\delta = \gamma - \alpha$:

$$\rho(T, p) = A\frac{p}{T^{\delta}}. \tag{10}$$

where the model constants A and δ have to be determined from the experimental data of **Table 1**. Using formula (10) and **Table 1** we have created error function Chi^2 which was minimized by the SOLVER program of the Excel package. The obtained results are as follows: $A = 0.121$ (mol K J^{-1}) and $\delta = 1.002$ (−). Note that $A^{-1} = 8.22$ (mol^{-1} $K^{-1}J$) reveals an approximation of the gas constant. Mentioned and illustrated above methodology for applications of the scaling and the gauge transformations will be applied to the following problems: self-similarity of hysteresis, self-similarity of total loss in SMM, multi-scaling of core losses in SMM, optimization of total loss in SMC and scaling conception of losses separation.

2. Self-similar model of hysteresis loop

The goal of the present section is to describe the self-similar mathematical model of hysteresis loop which enables us to express its self-similarity by the homogeneous function in general sense. Derivation of the model based on the well-known properties of tanh(·) suits for model of initial magnetization function [4]. It describes properly the saturation for both asymptotic values of the magnetic field $H \rightarrow \pm\infty$, as well as and the behaviour of magnetization in the neighbourhood of origin. However, this is too rigid for scaling. We make tanh(·) to be a softer by making the base of the natural logarithm free parameters [5]:

$$\tanh(x) -> \ tanH(a, b, c, d; x) = \frac{a^x - b^{-x}}{c^x + d^{-x}}. \tag{11}$$

where the bases have to satisfy the following conditions: $a > 1$, $b > 1$, $c > 1$, $d > 1$. These conditions guarantee correctness of the model; however, a little deviations from the mentioned constrains are possible.

First, we write down the model expression for initial magnetization curve:

$$M_P(X, \varepsilon) = M_0 P(X, \varepsilon);\ X \epsilon [0, X_{max}]. \tag{12}$$

where M_0 is magnetization corresponding to saturation expressed in tesla: [T], $X = \frac{H}{h}$, where H is magnetic field, and h is a parameter of the magnetic field dimension (A m^{-1}) to be determined. Function $P(X, \varepsilon)$ is of the following form:

$$P(X,\varepsilon)=\frac{a^{X-\varepsilon}-b^{-X+\varepsilon}}{c^{X-\varepsilon}-d^{-X+\varepsilon}} \tag{13}$$

where ε is modelling parameter related to θ, where $\varepsilon\ [-\frac{\theta}{2},\ +\frac{\theta}{2}]$. Let the upper and the lower branches of the hysteresis loop are of the following forms:

$$M_F(X,\theta)=M_0F(X,\theta);\ M_G(X,\theta)=M_0G(X,\theta). \tag{14}$$

where

$$F(X,\theta)=\frac{a^{X+\theta}-b^{-X-\theta}}{c^{X+\theta}-d^{-X-\theta}}\quad G(X,\theta)=\frac{a^{X-\theta}-b^{-X+\theta}}{c^{X-\theta}-d^{-X+\theta}}. \tag{15}$$

Let us consider for illustration the following symmetric example: $a = b = c = d = 4$ and $\theta = 1.3$, $\varepsilon = 0$, $M_0 = 1$ (See **Figure 1**).

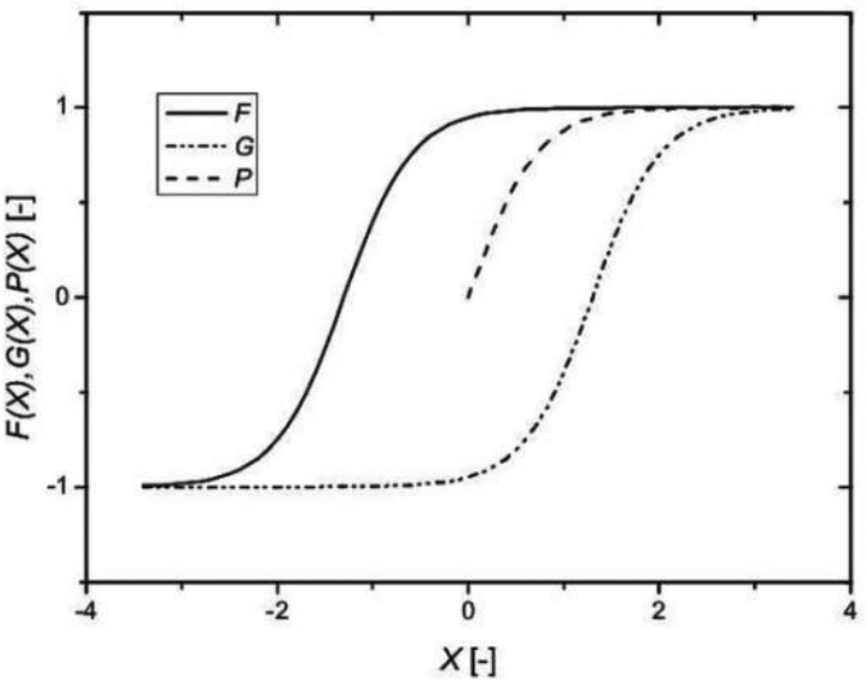

Figure 1. A model of nucleation-type hysteresis constructed with functions *F*, *P* and *G* according to (12)–(15).

Due to the asymptotic properties of magnetization, the functions $\boldsymbol{F(X, \theta)}$ and $\boldsymbol{G(X, \theta)}$ have to possess the same asymptotic properties. As we have mentioned, these components get equal values for $\boldsymbol{H \to \pm\infty}$. However, due to the uncertainty of measured magnitudes, it is possible to accept the saturation points at $X = X_{min}$ and $X = X_{max}$ being the end points of the hysteresis loop.

Therefore, the modelling process has to ensure that the initial function satisfies the following constrain:

$$|F(X_{max},\theta)-G(X_{max},\theta)|\leq|\psi|. \tag{16}$$

where $|\psi|=sup_X \frac{|M_F(X,\theta)-M_G(X,\theta)|}{M_0}$ is dimensionless measure of uncertainty corresponding to $|M_F(X)-M_G(X)|$.

The scaling in space of loops is performed by scaling each loop's component (13), (14), (15) and (16). For simplicity of further investigations, we consider simplified symmetric model, where all the bases of tanH( ) are equal:

$$\frac{M_F(X,\theta)}{M_0}=\frac{(a)^{X+\theta}-(a)^{-X-\theta}}{(a)^{X+\theta}+(a)^{-X-\theta}} \tag{17}$$

$$\frac{M_G(X,\theta)}{M_0}=\frac{(a)^{X-\theta}-(a)^{-X+\theta}}{(a)^{X-\theta}+(a)^{-X+\theta}} \tag{18}$$

$$\frac{M_P(X,\varepsilon)}{M_0}=\frac{(a)^{X+\varepsilon}-(a)^{-X-\varepsilon}}{(a)^{X+\varepsilon}+(a)^{-X-\varepsilon}} \tag{19}$$

Let us perform scaling on (17) and (18). Since exponents are dimensionless, the scaling on this level cannot be supported by dimension analysis. However, we are able to scale the following magnitudes a, $M_F(X, \theta)$, $M_G(X, \theta)$, $M_P(X, \theta)$, and to prove the following theorem:

For the symmetric model (17)–(19), the hysteresis loop is invariant with respect to scaling and gauge transformation [5]. Following definition of the homogeneous function in general sense (6), we write down the scaled form of the hysteresis loop:

$$\frac{M_F(X,\theta)}{M_0}\lambda^{\nu}=\frac{(\lambda^{\alpha}a)^{X+\theta}a^{\chi}-(\lambda^{\alpha}a)^{-X-\theta}a^{-\chi}}{(\lambda^{\alpha}a)^{X+\theta}a^{\chi}+(\lambda^{\alpha}a)^{-X-\theta}a^{-\chi}}, \tag{20}$$

$$\frac{M_G(X,\theta)}{M_0}\lambda^{\nu}=\frac{(\lambda^{\alpha}a)^{X-\theta}a^{\chi}-(\lambda^{\alpha}a)^{-X+\theta}a^{-\chi}}{(\lambda^{\alpha}a)^{X-\theta}a^{\chi}+(\lambda^{\alpha}a)^{-X+\theta}a^{-\chi}}, \tag{21}$$

where exponentials a^{χ} and $a^{-\chi}$ represent action of the gauge transformation. This formal trick guarantees proper order of actions: the first has to be performed scaling than after that gauge

http://dx.doi.org/10.5772/63285

transformation. According to the assumption just above (6), we are free to make the following substitution:

$$\lambda^{\alpha} = a^{p-1}, \tag{22}$$

where $p \epsilon \mathbb{R} \backslash 0$. Substituting (22) leads to the following forms of (20) and (21):

$$\frac{M_F(X,\theta)}{M_0} a^n = \frac{(a)^{p(X+\theta)+\chi} - (a)^{p(-X-\theta)-\chi}}{(a)^{p(X+\theta)+\chi} + (a)^{p(-X-\theta)-\chi}} \tag{23}$$

$$\frac{M_G(X,\theta)}{M_0} a^n = \frac{(a)^{p(X-\theta)+\chi} - (a)^{p(-X+\theta)-\chi}}{(a)^{p(X-\theta)+\chi} + (a)^{p(-X+\theta)-\chi}}. \tag{24}$$

where for abbreviation, we introduce $n = \frac{\nu}{\alpha}(p-1)$. Introducing the following new variables:

$$M_0' = a^{-n} M_0, X' = pX + \chi, \theta' = p\theta, \tag{25}$$

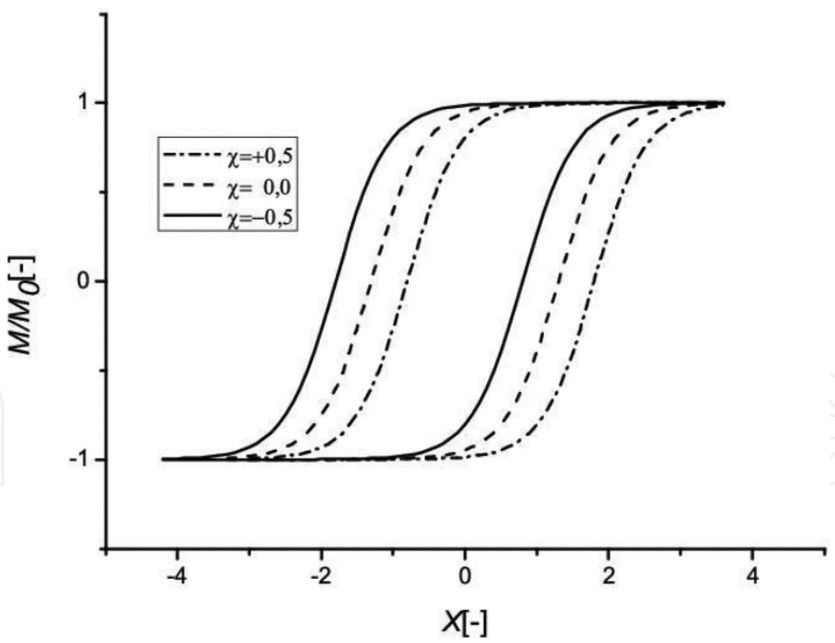

Figure 2. Magnetic hysteresis family for a=4, p=1, n=1, θ=1.3, $\frac{\nu}{\alpha}$=1.

we derive (17) and (18), which proves the considered thesis. The initial magnetization curve (19) is invariant with respect to scaling and gauge transformation as well. The proof goes the same way as for (17) and (18). Therefore, we can formulate conclusion that the presented model

of hysteresis loop is self-similar. Below in **Figures 2–4**, we present some examples of the hysteresis loops which may suggest how to apply the scaling and gauge transformation for modelling of hysteresis phenomena.

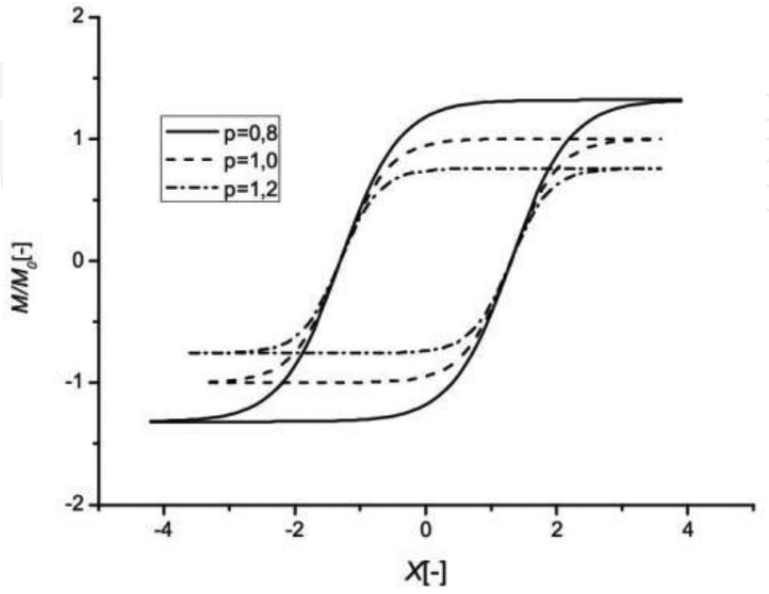

Figure 3. Magnetic hysteresis family for $a=4,\ \chi=0,\ n=1,\ \theta=1.3,\ \frac{v}{\alpha}=1$.

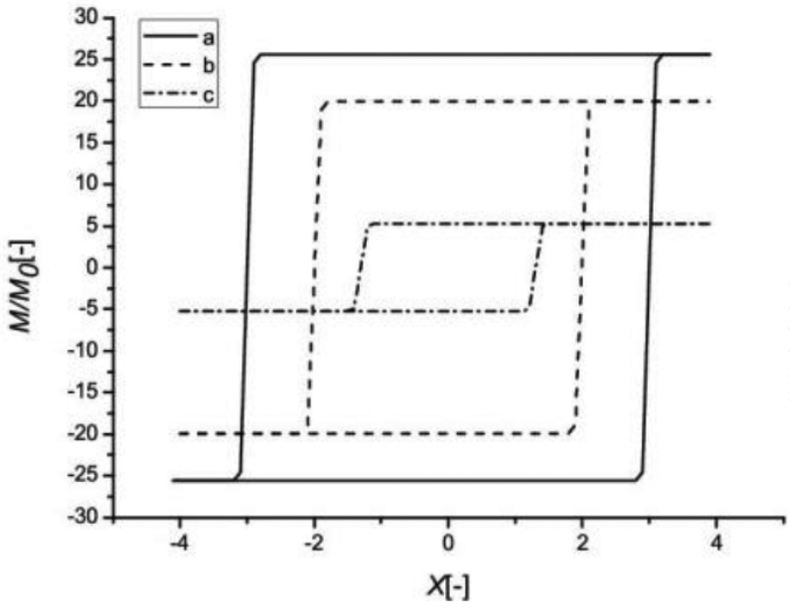

Figure 4. Magnetic hysteresis family for the following values of the model and scaling parameters: $(a)\ a=4,\ \theta=3,\ p=14,\ \frac{v}{\alpha}=-0.18,\ \chi=0,\ (b)\ a=4,\ \theta=2,\ p=13,\ \frac{v}{\alpha}=-0.18,\ \chi=0,$

$(c) a=4,\ \theta=1.3,\ \chi=0,\ (b)\ \theta=2,\ p=13,\ \frac{v}{\alpha}=-0.18,\ \chi=0.$

Figure 2 presents how the pure gauge transformations generate a displacement of transformed loops along the horizontal axis. **Figure 3** presents compression of loops along the vertical axis under the scaling. Finally, **Figure 4** presents the loop's family for large value of the scaling parameter p. Each element of this set resembles the Preisach hysteron [6, 7].

Multi-scaling of hysteresis loop. The derived above mathematical model of the hysteresis loop is not full. There is need to extend considered model with respect to frequency, pick of induction and temperature. As we have shown the loop's model is self-similar with respect to scaling of the following magnitudes X, M_0 and θ, these are as follows: dimensionless magnetic field, amplitude of magnetization and loop's closing parameter, respectively. By introducing new independent variables, we introduce new scales and corresponding new scaling parameters [8]. We have shown in [8, 9] that it is always possible to introduce a new characteristic scale; however, one must investigate whether the considered system possesses corresponding symmetry. This can be known only from investigations of the measurement data. In the considered model, there are two places where the new variables can be implemented. These are base of the tanH() function and the loop's closing parameter θ. There are many possible combinations for configurations of the new variables in presented model which can be applied:

$$(i)\left[B_m^{\beta'}a\left(\frac{f}{B_m^{\alpha'}},\frac{T}{B_m^{\gamma}}\right);B_m^{\beta'}\theta\left(\frac{f}{B_m^{\alpha'}},\frac{T}{B_m^{\gamma}}\right)\right];(ii)\left[B_m^{\beta}a\left(\frac{f}{B_m^{\alpha'}},\frac{T}{B_m^{\gamma}}\right);B_m^{\beta'}\theta(-)\right];(iii)\left[B_m^{\beta'}a\left(\frac{f}{B_m^{\alpha'}}\right);\theta(-)\right]. \quad (25a)$$

The list (25a) is not closed and can be extended as needed. We assume that $a(f, B_m, T)$ and $\theta(f, B_m, T)$ are homogenous functions in general sense. To simplify considerations, we chose for illustration the temperature less model (*iii*), where $\theta(-)$ is a constant. For the model of the function $a\left(\frac{f}{B_m^{\alpha'}}\right)$, we chose the square polynomial:

$$a = B_m^{\beta'}\left(\Gamma'_1\frac{f}{B_m^{\alpha'}}+\Gamma'_2\left(\frac{f}{B_m^{\alpha'}}\right)^2\right) \quad (25b)$$

where α', β', Γ'_1, Γ'_2 are model constants to be calculated from the measurement data, whereas the B_m pick of induction is correlated with X_{min} and X_{max}. Formulae (25b), (14) and (15) constitute frequency- and pick of induction-dependent loop model.

Equivalence classes and partitioning [10]. Transformation formulae (25) enable us to investigate algebraic structure of all the transformations which are composed of scaling and gauge transformation. Therefore, the whole set of p and the multiplication constitute $\mathcal{G}_p = \{\mathbb{R}\backslash 0, \cdot\}$ group. Moreover, $\forall a > 0$ and $\forall \frac{v}{\alpha} \neq 0$, the following expression $a^{(1-p)\frac{v}{\alpha}}$ represents an infinite number of groups being isomorphic to $\mathcal{G}_p$. Gauge transformations χ $\mathbb{R}$ and the addition constitute $\mathcal{G}_\chi = \{\mathbb{R}, +\}$ group. Each of revealed group possesses the own representation space. $\mathcal{G}_p$ group operates in the spaces generated by X, θ and M_0 *and* $\mathcal{G}_\chi$ group operates in the space

spanned by X variable. The considered model of loop reveals a combination of $\mathcal{G}_p$ and $\mathcal{G}_\chi$ which operates in space generated by (X, θ) pair. Therefore, total symmetry of the considered model can be presented in the following matrix representation (26):

$$\begin{bmatrix} p & 0 & 0 \\ 0 & a^{(1-p)\frac{v}{\alpha}} & 0 \\ 0 & 0 & p \end{bmatrix} \begin{bmatrix} X \\ M_0 \\ \theta \end{bmatrix} + \begin{bmatrix} \chi \\ 0 \\ 0 \end{bmatrix} = \begin{bmatrix} X' \\ M_0' \\ \theta_0' \end{bmatrix}. \tag{26}$$

Therefore, the total symmetry of the considered group has got the structure of the following semi-direct product $\mathcal{G}_G = (\mathcal{G}_p \times \mathcal{G}_{p'} \times \mathcal{G}_p) \ltimes \mathcal{G}_{\chi,0,0'}$ where $p' = a^{(1-p)\frac{v}{\alpha}}$ represents isomorphic mapping $\mathcal{G}_p \rightarrow \mathcal{G}_{p'}$. Let V_h be space of the all hysteresis' models represented by (14) and (15). Group element $g_{p,p',p,\chi} \epsilon \mathcal{G}_G$ is automorphism in V_h if $\forall\, v \epsilon V_h$ yields $g_{p,p',p,\chi} v \epsilon V_h$. Set of the all automorphisms G_A constitutes automorphism group, where $\mathcal{G}_A \subset \mathcal{G}_G$. Let us distinguish the loop $v_1 = \begin{bmatrix} X_1 \\ M_{01} \\ \theta_1 \end{bmatrix} \in V_h$, and relate v_1 with v_2:

$$v_1 \mathcal{R} v_2, \tag{26a}$$

where $\mathcal{R}$ means the binary relation given by (26).

Definition:

Equivalence binary relation on a set $V(h)$ is a relation, which is reflexive, symmetric and transitive [11]. Due to the group structure of $\mathcal{G}_{G'}$ (26a) satisfies these conditions and $\mathcal{R}$ is equivalence relation.

Let $\mathcal{R}$ be an equivalence relation on V_h, then $\mathrm{E_{v1}} \subset V_h$ containing all elements $v_2 \in V_h$ satisfying (26a) is called the equivalence class of v_1. The sets $\mathrm{E_{vi}}$ are pairwise disjoint, that is $\mathrm{E_{v_i}} \cap \mathrm{E_{v_j}} = \varnothing$ if $v_i \neq v_j$. Union of the all equivalence classes is the V_h space: $\cup_{v_i} E_{v_i} = V_h$. What practical use one may have from equivalence relations and partitioning. Let us assume the following $v_1 \mathcal{R} v_2$ relation, and then there exists a group element which relates both loops means that they are equivalent. However, in the opposite case, the two loops do not belong to a common class and then they are relevantly different from the algebra point of view.

3. Losses scaling in soft magnetic materials

Density of the total power losses in magnetic materials under variable magnetic field is due to eddy currents generated in the material. These may be generated for various scales of dimen-

sions: currents caused by Barkhausen jumps, what leads to a dependence $P_{hys} \propto (B^{1.6} f)$ [11], currents around moving domain walls $P_{exc} \propto (Bf)^{\frac{3}{2}}$ [12] and currents in the whole material volume $P_{clas} \propto (Bf)^2$ [11]. All of the aforementioned dependencies obey a power law, however, with a diverse value of exponents [13]. Therefore, one cannot talk about universality of the presented above formulae. However, certain universality of the power losses data of soft magnetic materials has been derived by applying the scaling. The proposed approach has been based on assumption that the density of the total power loss in soft magnetic materials was self-similar like intermittency of fully developed turbulent flow [1]. Moreover, using simple model of hysteresis loop (14), (15) and assuming semi-static conditions, we derive the following formula for the total power loss [14]:

$$P_{tot} = f\mu_0 M_0 h \quad a^{-n} ln\left(\frac{(a^{2\cdot(p\theta+pX_{max}+\chi)}+1)}{(a^{2\cdot(pX_{max}+\chi)}+a^{2p\theta})} \cdot \frac{\left(a^{2\cdot(pX_{min}+\chi)}+a^{2p\theta}\right)}{(a^{2\cdot\left(p\theta+pX_{min}+\chi\right)}+1)}\right) (p \cdot \ln(a))^{-1}. \tag{26b}$$

In case of the symmetric extrema of magnetic field $X_{min} = -X_{max}$, (26b) gets the following form:

$$P_{tot} = 4\theta f \mu_0 M_0 h a^{-n}. \tag{26c}$$

where a, $n = \frac{\nu}{\alpha}(p-1)$, $h = \frac{H}{X}$, θ and M_0 are the hysteresis loop parameters and μ_0 is the permeability of free space.

According to (26c), the formula for P_{tot} is monomial which is always self-similar mathematical expression. This theoretical result confirms experimental observations concerning homogeneity of P_{tot} in soft magnetic materials.

Let us assume that the density of the total power losses is homogenous function in general sense (6). Let P_{tot} (f, B_m) be density of the total power losses, where f and $B_m$are frequency and the pick of magnetic induction of flux waveform. Applying (6) for the two independent variables, we derive the most general form for P_{tot}:

$$P_{tot}\left(f, B_m\right) = B_m^{\beta} F\left(B_m^{-\alpha} f\right), \tag{27}$$

where α and β are scaling exponents and $F(\cdot)$ is an arbitrary function. These three unknown magnitudes have to be determined from experimental data. As the simplest approach to estimation of $F(\cdot)$, we have applied the Maclaurin expansion of (27):

$$P_{tot}\left(f, B_m\right) = B_m^{\beta}(\Gamma^{(1)}\left(B_m^{-\alpha} f\right) + \Gamma^{(2)}\left(B_m^{-\alpha} f\right)^2). \tag{28}$$

where $\Gamma^{(k)}=\frac{1}{k!}\Gamma^{(k)}(0)$. Since the total losses vanish for $f = 0$ or for $B_m = 0$, the constant term of expansion (28) equals zero.

3.1. Measurement data

The measurement of density of total power losses was carried out following the IEC Standards (60404-2, 60404-6). During measurements, the shape factor of secondary voltage was equal to 1.111± per cent. Extended uncertainty of obtained measurements was equal to about 0.5%. The measurements covered the three following classes of soft magnetic materials:

- Crystalline materials;
- Amorphous alloys, Co-based and Fe-based; and
- Nanocrystalline alloy.

Density of total power losses was measured as a function of the maximum induction $B_m \in [0.1]$ (T), 1.8(T)] at fixed values of $f \leq 400$ (Hz). Samples of conventional crystalline materials were strips, whereas the remaining ones had the shape of cylinder.

3.2. Estimation of expansion parameters (28) from measurement data

Magnetic materials	α(–)	β(–)	$\Gamma^{(1)}(m^2\mathrm{T}^{(\alpha-\beta)}/s^2)$	$\Gamma^{(2)}(m^2\mathrm{T}^{(2\alpha-\beta)}/s)$
GO—3% Si-Fe	−2.16	−1.19	12.78×10^{-3}	37.68×10^{-6}
$Co_{71.5}Fe_{2.5}Mn_2Mo_1Si_9B_{14}$	−1.55	−0.35	2.88×10^{-3}	1.90×10^{-6}
$Fe_{73.5}Cu_1Nb_3Si_{13.5}B_9$	−1.81	−0.70	0.17×10^{-3}	0.71×10^{-6}

Table 2. Values of scaling exponents α, β and values of amplitudes $\Gamma^{(k)}$.

Firstly, the initial values of exponents α, β and amplitudes $\Gamma^{(k)}$ were assumed and differences between all measurement values of density of total power losses and values of density of total power losses obtained from expansion (28) were calculated. Next, the Chi^2 function was optimized. Constraint of normal distribution of error was applied. Results of optimization for exponents α, β and amplitudes $\Gamma^{(k)}$ for chosen magnetic materials are given in **Table 2**.

The results, that is scaled values of the measurement data and the values obtained from the mathematical model, for the chosen magnetic materials, are shown in **Figures 5–7**, in the $\frac{P_{tot}}{B_m^{\beta}}$, $\frac{f}{B_m^{\alpha}}$ coordinates system. Based on the all results concerning the density of total power losses, the universal relationship between the scaling exponents α and β was stated. This relation is of the following form [15]:

$$\beta = 1.35\alpha + 1.75, \tag{29}$$

See also **Figure 8**. The origin of the relationship in (29) will be subject of further relations.

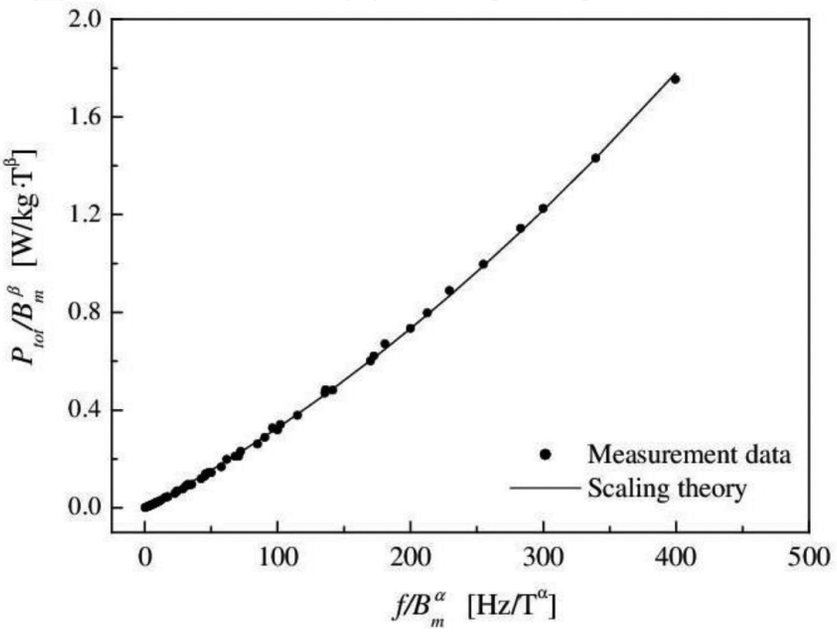

Figure 5. A comparison of measurement data of total density of power losses P_{tot} (markers) and values obtained from the scaling theory (solid line) for Co-based amorphous alloy $Co_{71.5}Fe_{2.5}Mn_2Mo_1Si_9B_{14}$.

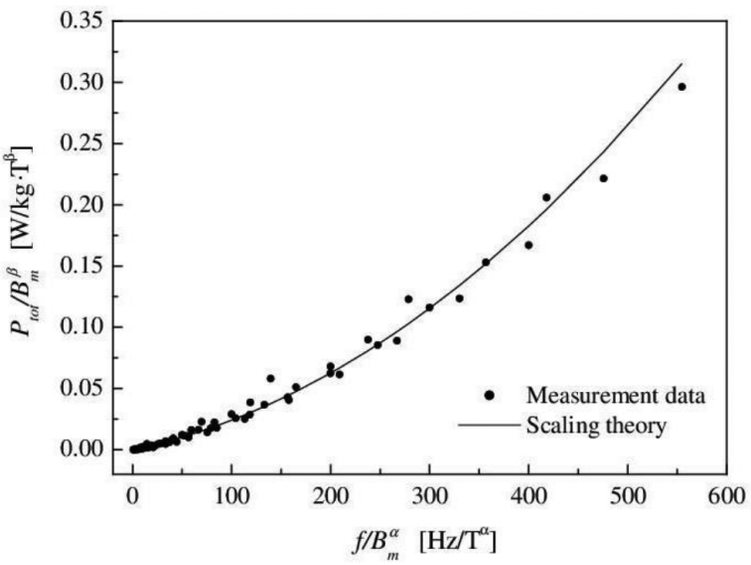

Figure 6. A comparison of measurement data of total density of power losses P_{tot} (markers) and values obtained from the scaling theory (solid line) for nanocrystalline alloy $Fe_{73.5}Cu_1Nb_3Si_{13.5}B_9$.

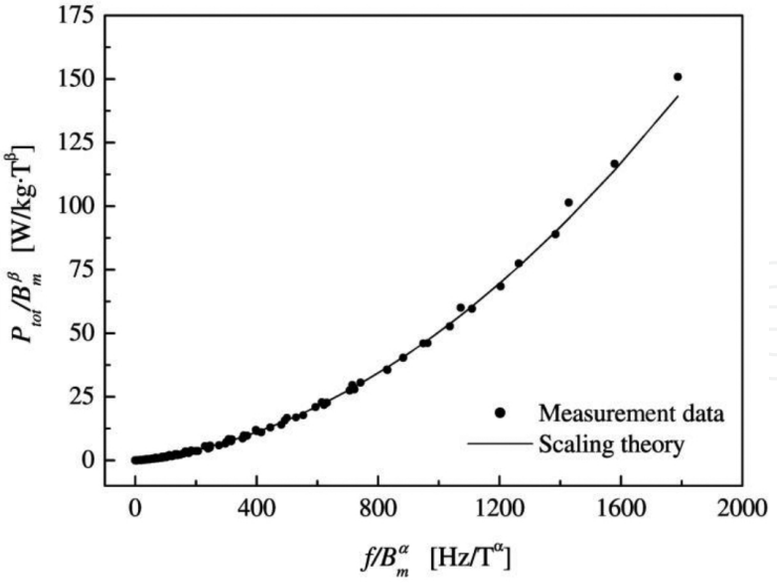

Figure 7. A comparison of measurement data for total density of power losses P_{tot} (markers) and values obtained from the scaling theory (solid line) for grain-oriented silicon steel 3% Si-Fe.

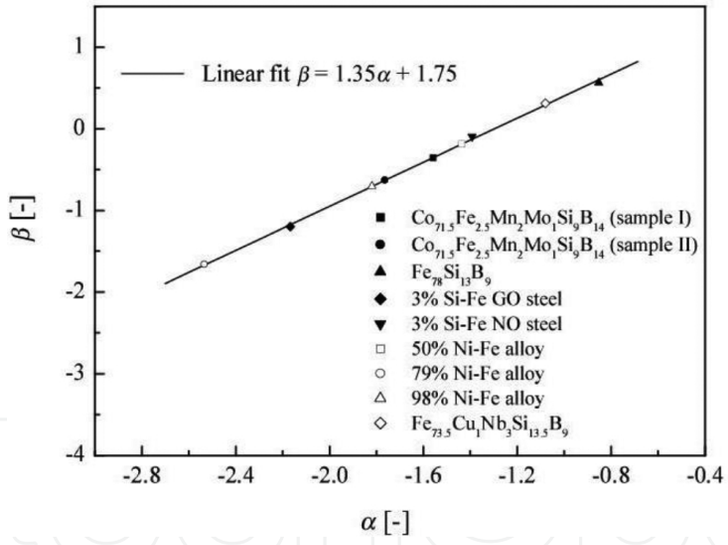

Figure 8. The universal relationship of the scaling exponents α and β. Markers correspond to estimations from experimental data, and continuous line corresponds to (29).

The three achievements resulting from scaling should be emphasized. The first one is a satisfactory agreement between the measurement data and the theoretical description. The second one is relation (29), which establishes the universal linear relationship between the scaling exponents and decreases the number of free parameters. The third achievement consists in revealing the data collapse. **Figures 5–7** are drawn in $\frac{P_{tot}}{B_m^{\beta}}$, $\frac{f}{B_m^{\alpha}}$ coordinates system and present the continuous sets of the losses characteristics of different values of B_m collapsed

just to a single curve. This effect is called "a single-sample data collapse" Reversible procedure $(\frac{P_{tot}}{B_m^{\beta}}, \frac{f}{B_m^{\alpha}}) \rightarrow (P_{tot}, f)$ splits the collapsed curves to separate curves for different values of B_m. This effect will be demonstrated for more complicated case (see **Figure 14**). Therefore, the scaling can be also applied as method for a compression of data. All examples in **Figures 5–7** present the single-sample data collapses. Having data for different materials and introducing for each of them are the following dimensionless magnitudes:

$$\tilde{P}_{tot} = \frac{\Gamma^{(2)}}{\Gamma^{(1)^2}} \frac{P_{tot}}{B_m^{\beta}} \quad \tilde{f} = \frac{\Gamma^{(2)}}{\Gamma^{(1)}} \frac{f}{B_m^{\alpha}}, \tag{30}$$

We obtain the multi-sample data collapse (see **Figure 9**). These results confirm the assumption of density of total power losses scaling. Applying these transformations to (28), we derive the dimensionless low for the density of power losses in soft magnetic materials:

$$\tilde{P}_{tot} = \tilde{f} + \tilde{f}^2. \tag{31}$$

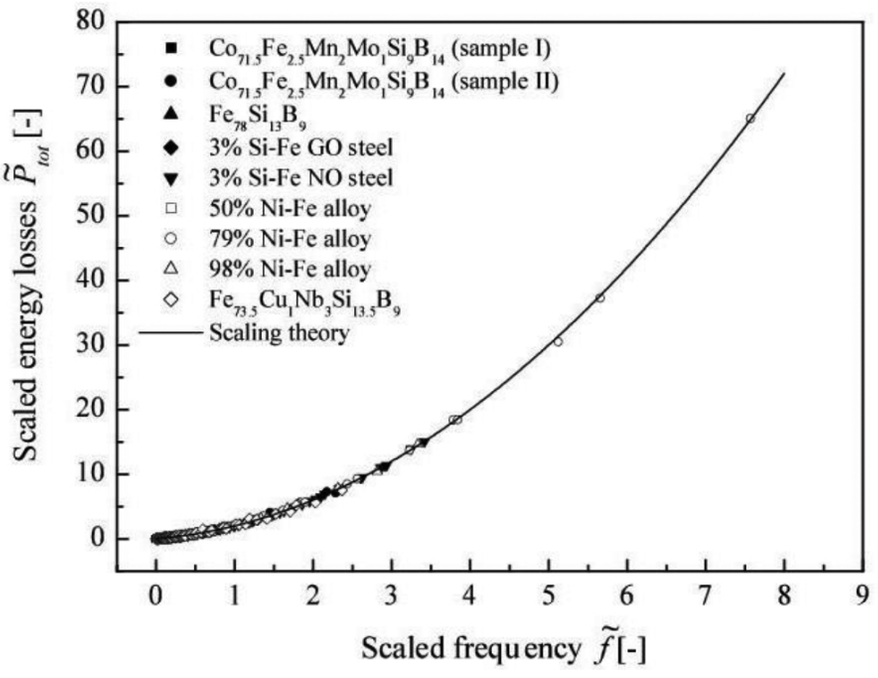

Figure 9. The multi-sample data collapse for total density of power losses $\tilde{P}_{tot}$ (markers) and values obtained from the scaling theory (solid line).

3.3. An application of the multi-sample data collapse

Mostly, the data collapse is applying as a tool for the detection of self-similarity. Here, we present a new application which solves problem of comparison measurements taken in

different laboratories [16]. In 1995, the leading European Laboratories busy with measurements of the electrical steel magnetic properties were trying to compare the measurement results of the power loss in electrical sheet steel under the conditions of rotating and alternating flux [17]. Taking from [17] the idea of the inter-comparison of measurement data of the energy losses in soft magnetic materials, we perform such an inter-comparison with data taken in two laboratories [16, 18], however, under the conditions of axial and alternating flux. Self-similarity of the density power losses enables us to scale off the interference of the sample's geometry and the material type from the dependence of power losses versus the pick of induction and magnetizing frequencies. This property of SMM allows comparing different measurement sets. Successively, this fact allows introducing an absolute measure of uncertainty characterizing the given measurement set. Therefore, the way for assessing the uncertainty contributions would not interfere with the abovementioned data comparison. Formula (30) suits very well to the mentioned above phenomena and constitute background for solution of the presented problem.

For inter-comparison, we have selected two sets of power losses data. The first one belongs to Yuan [18] and consists of the following three sets of data: $S_1=Fe_{76}Mo_2Si_2P_{10}C_{7.5}B_{2.5}$, $S_2=Fe_{79.8}Mo_{2.1}Si_{2.1}P_8C_6B_2$, $S_3=Fe_{80}Mo_1Si_2P_8C_6B_3$. The samples were thin ribbons wound into toroids. For details concerning measurement methods, we refer readers to [18]. On the basis of measured data, the parameters' values of (28) have been estimated (see **Table 3**, after [18]).

Sample	α(–)	β(–)	$\Gamma^{(1)}$(m^{2}T$^{(\alpha-\beta)}$s^{-2})	$\Gamma^{(2)}$(m^{2}T$^{(2\alpha-\beta)}$s^{-1})
S_1	−1.533	−0.319	6.744×10^{-3}	1.322×10^{-6}
$S2$	−0.364	1.259	1.412×10^{-2}	1.917×10^{-6}
$S3$	−0.504	1.069	9.11×10^{-3}	3.389×10^{-6}
$P1$	−2.945	−1.776	2.90×10^{-3}	4.60×10^{-6}
$P2$	−1.519	−0.375	2.53×10^{-3}	6.79×10^{-6}
$P3$	−3.231	−1.365	3.22×10^{-4}	1.95×10^{-7}

*The data for $S1$, $S2$ and $S3$ have been kindly supplied by the authors of Yuan et al. [18].

Table 3. Scaling exponents and coefficients of (28).

The second set contains some of our results [15, 19] for the power losses in the following alloys: amorphous ribbon $P_1=Fe_{7.8}Si_{13}B_9$, Co-based amorphous alloy $P_2=Co_{71.5}Fe_{2.5}M_{n2}M_{o1}Si_9B_{14}$ and nanocrystalline alloy $P_3=Fe_{73.5}Cu_1Nb_3Si_{15.5}B_7$. The corresponding scaling exponents α, β and the scaling coefficients $\Gamma^{(1)}$, $\Gamma^{(2)}$ are presented in **Table 3**.

Plotting $\widetilde{P}_{tot}$ versus $\widetilde{f}$ for the all considered samples (**Figure 10**), we confirm that the data collapse takes place for the selected samples.

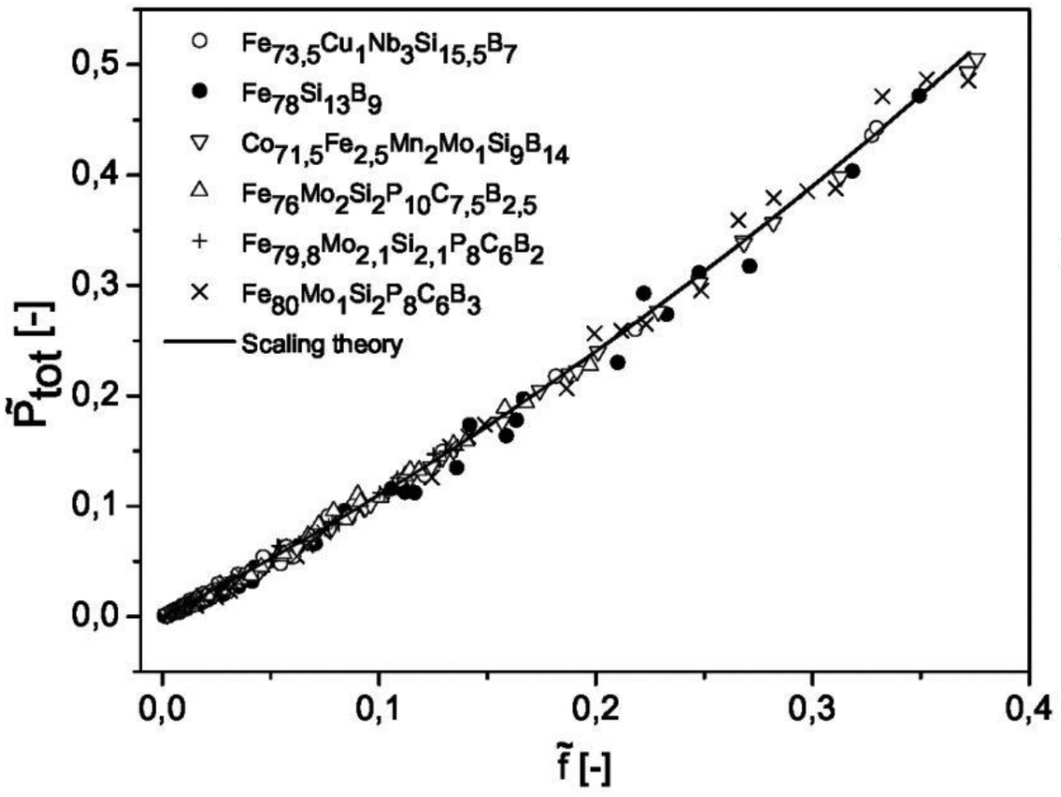

Figure 10. The data collapse for total power losses of compared materials.

Since all the magnitudes in (31) are dimensionless and the formula for $\tilde{P}_{tot}$ is sample independent, we propose to introduce a measure of uncertainty characterizing the measurement set by the total distance of all empirical points from the scaling curve (31):

$$D = \sqrt{\frac{1}{N}\sum_{i=1}^{N}\left(\tilde{P}_{tot}^{\exp}(\tilde{f}_i) - \tilde{P}_{tot}^{th}(\tilde{f}_i)\right)^2}, \tag{32}$$

where $\tilde{P}_{tot}^{exp}$, $\tilde{P}_{tot}^{th}$ are the power losses, measured and calculated from formula (31), $\tilde{f}_i$ is dimensionless frequency, where index *i* is running through the whole series of experimental data and N denotes length of the measured series. We consider the two sets of experimental data $\mathbb{S}$ and $\mathbb{P}$ corresponding to different LABs. Each set consists of the three series which correspond to different samples. To create effective measure of uncertainty characterizing measurement set of the given LAB, we calculate average measure $D_{av}$for the three samples belonging to either of two selected sets:

$$D_{av}^2 = \sum_{i=1}^{3}\frac{N_i}{N_1 + N_2 + N_3}D_i^2. \tag{33}$$

Comparisons of uncertainty measures are presented in **Table 4**.

Sample	N_i	$D_i^2(-)$	$\sqrt{D_{av}^2}(-)$
S_1	48	1.64×10^{-5}	8.11×10^{-3}
S_2	40	7.42×10^{-3}	
S_3	32	1.29×10^{-4}	
P_1	48	9.23×10^{-5}	6.53×10^{-3}
P_2	47	2.05×10^{-5}	
P_3	49	1.53×10^{-5}	

Table 4. Comparisons of uncertainty measures.

Progress in modern technologies depends on the comprehensive knowledge of material properties under standard and non-standard conditions. However, an agreed standardized method does not exist, and the reproducibility of the different methods used in different laboratories is unknown. We are of the opinion that the reason of such situation is lacking of statistical method enabling the appropriate data's inter-comparison. In this section, we have proposed a solution of this problem. As we have shown, the data collapse supplies method that enables us to introduce universal measure of uncertainty, which compares different experimental sets even based on different measurement methods. Therefore, the introduced method also can serve as a tool to compare measurement data obtained in different laboratories. The measure (33) expresses the total uncertainty characterizing the data set for the chosen range of dimensionless frequency $\tilde{f}$. There are four contributions to D_{av}resulting from the following: (1) uncertainty characterizing the measurement method and construction of the measurement set, (2) uncertainty of measurements of elementary magnitudes, (3) errors resulting from the approximation (28) and uncertainty of estimations of α, β, $\Gamma^{(1)}$ and $\Gamma^{(2)}$. The derived method is universal and can be applied to investigations of any phenomenon satisfying the self-similarity conditions.

4. Multi-scaling of core losses in soft magnetic materials

The application of soft magnetic materials in electronic devices requires knowledge of the losses under different excitation conditions: sinusoidal and non-sinusoidal flux waveforms of different shapes, with and without DC bias. Scaling theory allows the total power losses density to be derived in the form of a general homogeneous function, which depends on the peak to peak of the magnetic inductance ΔB, frequency f, DC bias H_{DC} and temperature T:

$$P_{tot} = F(f, \Delta B, H_{DC}, T). \tag{34}$$

The form of this function has been generated through the Maclaurin expansion with respect to scaled frequency. The parameters of the model consist of expansion coefficients, scaling exponents, parameters of DC bias mapping, parameters of temperature factor and tuning exponents. Values of these model parameters were estimated on the basis of measured data of total power density losses. However, influence of the DC bias on the self-similarity of measurement data was very relevant. In order to apply scaling to (34), the right-hand side has to be a homogeneous function in a general sense. This assumption has to be satisfied both by the experimental data and by the mathematical model. However, according to the results given in [20], Eq. (34) and measurement data are not uniform in the required sense when there is a DC bias. This problem has been solved by using the method invented by Van den Bossche and Valchev [21]. Their method consists in mapping of magnetic field into a pseudo-magnetization by using tanh(·):

$$P_{tot} = F(f, \Delta B, \tanh(H_{DC} \cdot c_0), T). \tag{35}$$

Following Bossche and Valchev, we have applied series of the mappings as expansion coefficients for modelling $F(\cdot,\cdot,\cdot,\cdot)$ function of (35):

$$H_{DC} \to [M_0, M_1, M_2, M_3]. \tag{36}$$

where $M_i = \tanh(H_{DC} c_i)$, where c_i are expansion coefficients, to be determined from measurement data.Therefore, applying definition for the homogeneous function in general sense, we have formulated the following scaling hypothesis: $\exists \{a, b, c, d, \mathrm{g}\} \in \mathbb{R}^5 : \forall \lambda \in \mathbb{R}_+$ yields: $P_{tot}(\lambda^a f, \lambda^b(\Delta B), \lambda^c[M_0, M_1, M_2, M_3], \lambda^d T) = \lambda^g P_{tot}(f, \Delta B, [M_0, M_1, M_2, M_3], T)$. Substituting the following $\lambda = (\Delta \mathrm{B})^{-1/b}$, we derive the most general form for P_{tot}which satisfies above hypothesis:

$$P_{tot} = (\Delta B)^{\beta} F\left(\frac{f}{(\Delta B)^{\alpha}}, \frac{[M_0, M_1, M_2, M_3]}{(\Delta B)^{\gamma}}, \frac{T}{(\Delta B)^{\delta}}\right). \tag{37}$$

where $\alpha = \frac{a}{b}$, $\beta = \frac{\mathrm{g}}{b}$, $\gamma = \frac{c}{b}$, $\delta = \frac{d}{b}$ are effective scaling exponents. $F(\cdot,\cdot,\cdot)$ is an arbitrary function of the three variables. Both the effective exponents and the F function have to be determined.

General formula (37) enables us to construct mathematical model which maps the four-dimensional space spanned by *f, ΔB, DC bias* and *T* into the one-dimensional P_{tot}space. In the first step, we separate the temperature factor $\Theta(\cdot)$:

$$F\left(\frac{f}{(\Delta B)^{\alpha}},\frac{[M_0,M_1,M_2,M_3]}{(\Delta B)^{\gamma}},\frac{T}{(\Delta B)^{\delta}}\right)=\Phi\left(\frac{f}{(\Delta B)^{\alpha}},\frac{[M_0,M_1,M_2,M_3]}{(\Delta B)^{\gamma}}\right)\Theta\left(\frac{T}{(\Delta B)^{\delta}}\right). \tag{38}$$

Let us assume that $\Phi(\cdot,\cdot)$ consists of two terms which need not be independent. However, the second one is H_{DC} dependent in contrary to the first one. For both of them, we assume the Maclaurin expansions with respect to scaled frequency $f/(\Delta B)^{\alpha}$, which is very much suited for the Bertotti decomposition. Moreover, the first term should describe losses for $H_{DC}\rightarrow 0$, whereas the second term must vanish for this condition. The resulting expression takes the following form:

$$\Phi\left(\frac{f}{(\Delta B)^{\alpha}},H_{DC}\right)=\Sigma_{i=1}^{4}\Gamma_i\left(\frac{f}{(\Delta B)^{\alpha}}\right)^{i}+\Sigma_{i=0}^{3}\Gamma_{i+5}\left(\frac{f}{(\Delta B)^{\alpha}}\right)^{i}\frac{\tanh(H_{DC}\cdot c_i)}{(\Delta B)^{\gamma}}. \tag{39}$$

Since (39) has been created by the Maclaurin expansion, all series exponents are integers. However, it may be so that the best error's minimum is obtained for fractional values of exponents. For this purposes, we introduce tuning exponents x and y:

$$\Phi\left(\frac{f}{(\Delta B)^{\alpha}},H_{DC}\right)=\Sigma_{i=1}^{4}\Gamma_i\left(\frac{f}{(\Delta B)^{\alpha}}\right)^{i(1-x)}+\Sigma_{i=0}^{3}\Gamma_{i+5}\left(\frac{f}{(\Delta B)^{\alpha}}\right)^{(i+y)(1-x)}\frac{\tanh(H_{DC}\cdot c_i)}{(\Delta B)^{\gamma}}. \tag{40}$$

On the basis of some numerical test simulations, we have selected the following Padé approximant for $\Theta(\cdot)$:

$$\Theta=\left(\frac{\psi_0+\theta(\psi_1+\theta\psi_2)}{1+\theta(\psi_3+\theta\psi_4)}\right)^{1-z} \tag{41}$$

where $\theta=\frac{T+\tau}{\Delta B^{\delta}}$ is gauged and scaled temperature, T is measured temperature in °C, z *is* tuning parameter, and ψ_i are Padé approximant coefficients. After all improvements of $F(\cdot,\cdot,\cdot)$, the final form is still homogenous function in general sense (6).

In order to perform core loss measurements, the *B-H* loop measurement has been evaluated as the most suitable. This technique enables rapid measurement while retaining a good accuracy. The measurement set works in the following way: two windings are placed around the core under test. Taking into account the number of secondary winding turns and the effective core cross section, the secondary winding voltage V is integrated into the core flux density B. Next taking into account the number of primary winding turns and the effective magnetic path length of the core under test, the magnetic field strength H is calculated.

Then, the total power losses per unit volume is the enclosed area of the *B-H* loop multiplied by the frequency *f*. The test system consists of a power stage, a power supply, an oscilloscope and a heating chamber. It is controlled by a MATLAB program running on a PC computer under Microsoft Windows. The power stage is capable of a maximum input voltage of 450 V, output current of 25 A and a switching frequency of up to 200 kHz. The *B-H* loop measurements have been performed for SIFERRIT. The rectangular voltage shape across the core and DC bias has been applied, while the duty cycle was 50%.

The tested core data were as follows:

- Material name: EPCOS N87

- Core shape: toroid R42

- Number of primary windings: 10

- Number of secondary windings: 5

- Magnetic path length [mm]: 354

- Cross section [mm^2]: 840

The following factors influence the accuracy of measurements:

- Phase shift error of voltage and current <4%

- Equipment accuracy <5.6%

- Capacitive couplings negligible (capacitive currents are relatively lower compared to inductive currents)

- Temperature <4%.

A	**β**	**δ**	**Γ_1**	**Γ_2**	**Γ_3**	**Γ_4**	**Γ_5**
−11.63	−8.64	−0.179	−1.408	739.5	1253.4	4238.5	0.123
Γ_6	Γ_7	Γ_8	c_0	c_1	c_2	c_3	γ
−30.97	−51.87	−4201.4	−0.488	−2.44E-02	−0.181	0.165	0.00
T	ψ_1	ψ_2	ψ_3	ψ_4	ψ_5	x	y
7.77E-02	−0.899	2.397	14.45	−1.27E-01	0.283	0.526	0.289
z							
4.84E-02							

Table 5. The set of estimated model's parameters of (37)–(41).

T	ΔB	f	H_{DC}	P_{tot}	T	ΔB	f	H_{DC}	P_{tot}
[°C]	[T]	[kHz]	[A/m]	[Wm^{-3}]	[°C]	[T]	[kHz]	[A/m]	[Wm^{-3}]
28.1	0.395	1	8.634	4064.3	28.1	0.391	1	20.146	4469.0
28.1	0.374	1	60.634	6332.4	28.3	0.351	1	86.651	6463.6
17.7	0.398	2	7.801	9452.1	17.8	0.398	2	20.555	10663.8
18.9	0.396	2	35.583	12745.8	18.5	0.377	2	89.240	16015.6
26.2	0.400	5	6.570	21131.3	26.4	0.4	5	17.820	23110.0
26.5	0.398	5	33.230	28057.3	27.1	0.386	5	89.400	35209.8
28.4	0.401	10	5.892	41549.0	28.6	0.401	10	17.477	45257.9
28.8	0.400	10	31.820	54650.9	29.7	0.393	10	73.960	63821.6
30.8	0.386	10	105.000	64632.1	28.4	0.49	1	11.694	6611.0
28.4	0.488	1	24.299	7196.0	28.4	0.451	1	78.390	8771.6
19.1	0.497	2	10.120	15234.1	19.2	0.496	2	23.718	16781.0
19.3	0.485	2	54.630	19235.9	19.8	0.475	2	76.860	20100.2
27.7	0.502	5	8.920	34634.8	27.4	0.503	5	15.020	36195.2
27.7	0.501	5	21.500	37496.6	28.6	0.496	5	47.500	41259.7
31.7	0.499	10	20.520	71226.8	32.2	0.494	10	45.040	76876.5
32.6	0.487	10	67.140	80858.2	28.5	0.588	1	14.420	10042.9
28.7	0.561	1	57.970	11239.6	28.7	0.541	1	78.080	11255.7
29.1	0.580	2	12.820	19689.9	28.7	0.576	2	54.360	22043.0
30.1	0.592	5	42.400	52126.7	31.1	0.599	10	10.290	92648.6
31.3	0.595	10	31.230	96446.4	28.9	0.684	1	22.050	14150.5
28.1	0.389	1	33.507	5358.8	28.4	0.346	1	91.066	6376.4
18.2	0.386	2	68.034	15049.1	18.7	0.367	2	110.590	16027.7
26.8	0.394	5	58.800	32614.3	27.5	0.386	5	97.779	35945.6
29.2	0.396	10	61.172	62814.4	30.2	0.387	10	99.190	64410.1
28.3	0.473	1	54.300	8296.5	28.5	0.443	1	85.100	8702.4
19.7	0.480	2	68.360	20073.3	20.2	0.469	2	87.440	20547.5
28.1	0.500	5	31.420	39530.2	31.5	0.499	10	7.570	65879.7
27.3	0.501	5	15.030	36194.3	28.5	0.58	1	36.010	10790.0
28.7	0.586	2	33.490	21002.2	30.2	0.616	5	36.050	54344.9
34.7	0.586	10	61.250	96583.3	29.0	0.669	1	41.330	14417.5

Table 6. Selected 60 records of the measurement data of SIFERRIT N87.

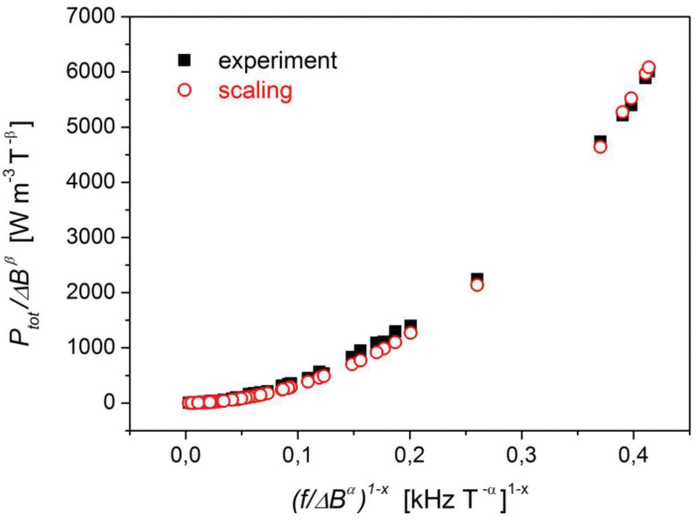

Figure 11. Projection of the measurement points and the scaling theory points (38)–(41) in $((\frac{f}{\Delta B^{\alpha}})^{(1-x)}, P_{tot}/\Delta B^{\beta})$ plane.

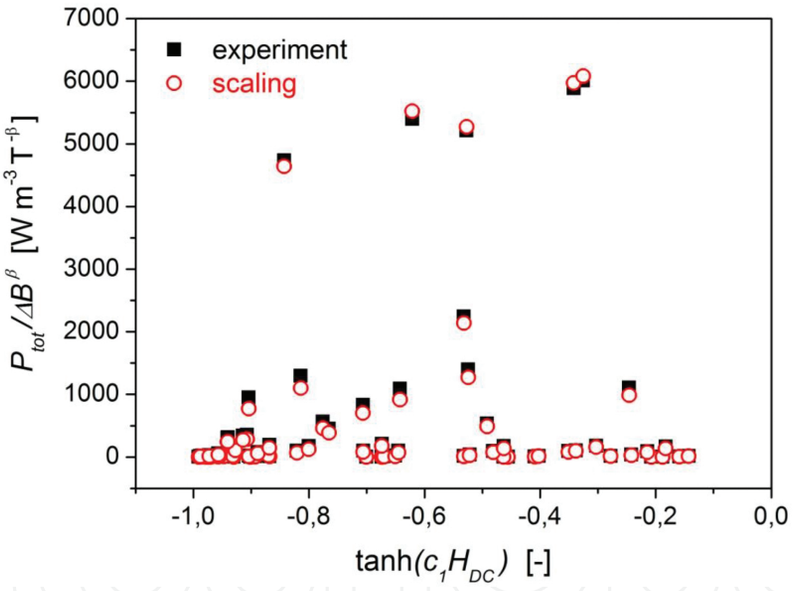

Figure 12. Projection of the measurement points and the scaling theory points (38)–(41) in ((tan $h(c_1 H_{DC})$, $P_{tot}/\Delta B^{\beta}$) plane.

Some comments concerning temperature change/stabilization have to be done. For details of the applied measurement method and the errors of the relevant factors, we refer to [22, 24]. The parameter values of (37)–(41) have been estimated by minimizing χ^2 of our experimental data and using the simplex method of Nelder and Mead [23]. The measurement series consists of 60 points (see **Table 5**). The standard deviation per point is equal to 15 Wm^{-3}. Applying the formulae (37)–(41) and the estimated parameter values (**Table 6**), we have drawn the three scatter plots given in **Figures 11–13**, which compare estimated points those obtained through

experimentation in the three projections, respectively. Note that in order to ensure numerical stability during the estimation process, the unit of frequency was set at 1 kHz, while other magnitudes were expressed in the SI unit system.

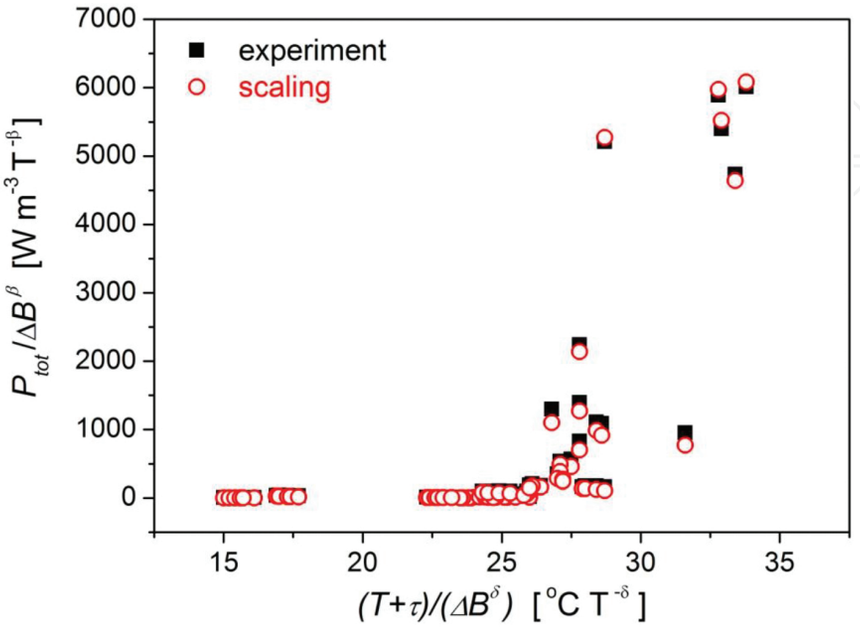

Figure 13. Projection of the measurement points and the scaling theory points (38)–(41) in $((T+\tau)/\Delta B^{\delta}, P_{tot}/\Delta B^{\beta})$ plane.

Scaled variables $P_{tot}/(\Delta B)^{\beta}$ and $f/(\Delta B)^{\alpha}$ are very convenient for the model parameter estimations. By using these variables, the number of independent variables is reduced. Also the collapsed form of power losses characteristic is very compact and easy to implement. However, for the purpose of designing of magnetic circuits, it is necessary to have the split characteristics which describe the physical magnitude P_{tot}versus the physical ones: T, f, H_{DC} and ΔB. Note that formula (37) is suitable just for this task. Let us assume the characteristics family for the following values of the independent variables: T, f, H_{DC} and $T=30\,°\mathrm{C}$, $H_{DC}=7\frac{A}{m}$, $\Delta B=\in\{0.4-0.7\}\mathrm{T}$, and $f=\in\{0.0-10.0\}\mathrm{kHz}$. Using (37) and applying (38)–(41) as well as **Table 6**, we derive the characteristics presented in **Figure 14**.

The efficiency of scaling in solving problems concerning power losses in soft magnetic material has already been confirmed in recent papers [15, 25]. However, this paper is the first one which presents an application of scaling in modelling the temperature dependence of the core losses. The presented method is universal, which means that it works for a wide spectrum of excitations and different soft magnetic materials. Moreover, the presented model formulae (37)–(41) are not closed and can be adapted for a current problem by fitting the forms of both factors Φ and Θ. Ultimately, one must say that the degree of success achieved when applying the scaling depends on the property of the data. The data must obey the scaling.

http://dx.doi.org/10.5772/63285

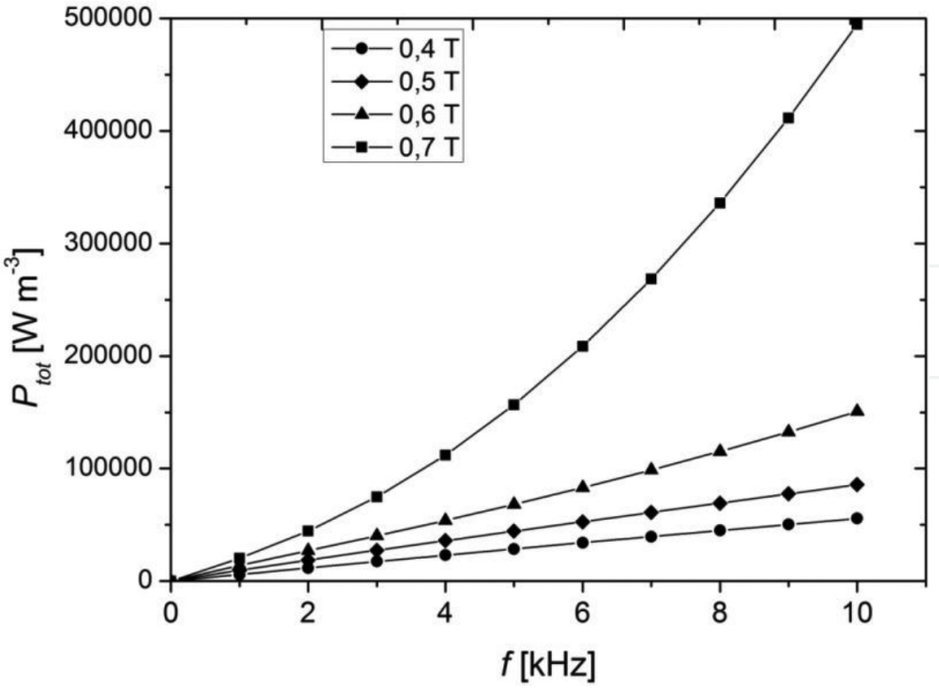

Figure 14. Family of the power losses characteristics P_{tot} versus frequency f derived for SIFERRIT N87 material for $T=30°\mathrm{C}$, $H_{DC}=7\frac{A}{m}$.

5. Optimization of power losses in soft magnetic composites

Recently, novel concept of technological parameters' optimization has been applied in soft magnetic composites (SMCs) by Ślusarek et al. [26]. This concept is based on the assumption that power losses in SMC obey the scaling law. The efficiency of this approach has been confirmed in [9]. The scaling is very useful tool due of the three reasons:

- It reduces number of independent variables f and B_m to the effective one f/B_m^{α},
- Determines general form of losses of power characteristic in a form of homogenous function in general sense, and
- Determines general form of losses of power characteristics in a form of different dimensions.

Therefore, applying concept of the homogenous function in general sense, we apply the following expansion:

$$\frac{P_{tot}}{B_m^{\beta}}=\left(f/B_m^{\alpha}\right)\cdot\left(\Gamma_1+f/B_m^{\alpha}\cdot\left(\Gamma_2+f/B_m^{\alpha}\cdot\left(\Gamma_3+f/B_m^{\alpha}\cdot\Gamma_4\right)\right)\right). \tag{42}$$

Γ_n, α and β parameters have been estimated for different values of pressure and temperature [9]. For the purpose of this paper, we take into account only one family of power losses

characteristics which are presented in **Figures 15** and **16**. The corresponding estimated values of the model parameters are presented in **Table 7**. For all other details concerning SMC material and measurement data, we refer to [9]. Now we are ready to formulate the goals of this section. Main goal is to describe minimization of the power losses in SMC by using model density of power losses (42) and corresponding values of the model parameters. From the first row of **Table 7**, we can see that dimensions of the Γ_n coefficients depend on the values of α and β exponents. Therefore, the power losses characteristics presented in **Figures 15** and **16** are different dimensions. So, we have to answer the following question: Are we able to relate them in the optimization process which has been described in [9, 26]?

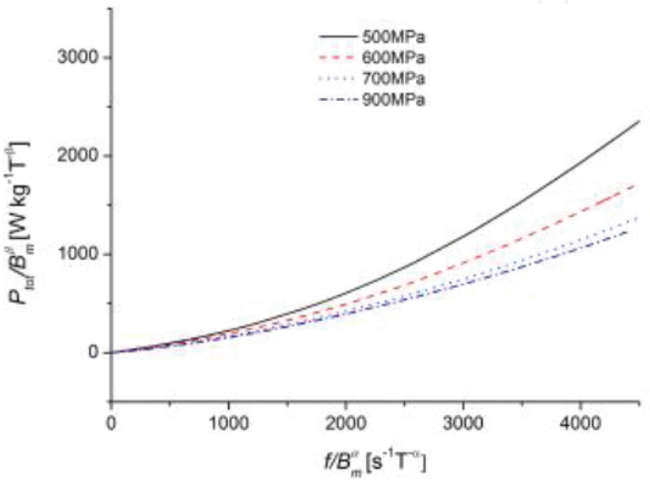

Figure 15. Selection of the power losses characteristics $P_{tot}/(B_m)^{\alpha}$ versus $f/(B_m)^{\alpha}$ calculated according to (42) and **Table 1** for Somaloy 500 [26], T = 500°C.

In this section, we show that if the considered characteristics obey the scaling, then the binary relation between them is invariant with respect to this transformation and comparison of two magnitudes of different dimensions has mathematical meaning. Reach measurement data of power losses in Somaloy 500 have been transformed into parameters of (42) versus hardening temperature and compaction pressure (**Table 7**) in [26]. Information contained in this table enables us to infer about topological structure of set of the power losses characteristics and finally to construct pseudo-state equation for SMC and derive new algorithm for the best values of technological parameters.

Scaling of binary relations. Let the power losses characteristic has the form determined by the scaling (27). It is important to remain that α and β are defined by initial exponents a, b and c (see after formula (27)):

$$\alpha = \frac{a}{b}; \beta = \frac{c}{b}. \tag{43}$$

Let us concentrate our attention at the point on the $\frac{f}{B_m^{\alpha}}$ axis of **Figures 15** or **16**:

http://dx.doi.org/10.5772/63285

$$\frac{f}{B_m^{\alpha}} = \frac{f_1}{B_{m1}^{\alpha 1}} = \frac{f_2}{B_{m2}^{\alpha 2}} = \frac{f_3}{B_{m3}^{\alpha 3}} = \frac{f_4}{B_{m4}^{\alpha 4}}. \tag{44}$$

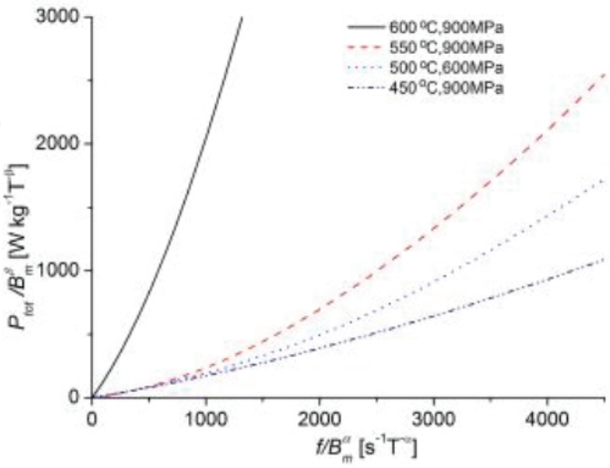

Figure 16. Selection of the power losses characteristics $P_{tot}/(B_m)^{\alpha}$ versus $f/(B_m)^{\alpha}$ calculated according to (42) and **Table 1** for Somaloy 500 [26].

Let us take into account the two characteristics and let us assume that

$$\frac{P_{tot1}}{B_{m1}^{\beta 1}} > \frac{P_{tot2}}{B_{m2}^{\beta 2}}. \tag{45}$$

T	p	α	β	Γ_1	Γ_2	Γ_3	Γ_4
[°C]	[MPa]	[–]	[–]	[m^2 s^{-2}T$^{\alpha-\beta}$]	[m^2 s^{-1}T$^{2\alpha-\beta}$]	[m^{2}T$^{3\alpha-\beta}$]	[m^2 sT$^{4\alpha-\beta}$]
500	500	−1.312	−0.011	0.171	3.606×10^{-5}	1.953×10^{-8}	-2.255×10^{-12}
500	600	−1.383	−0.125	0.153	3.328×10^{-5}	9.254×10^{-8}	-1.177×10^{-12}
500	700	−1.735	−0.517	0.156	2.393×10^{-5}	2.309×10^{-8}	-8.075×10^{-14}
500	900	−1.395	−0.082	0.101	6.065×10^{-5}	-8.031×10^{-8}	7.877×10^{-13}
400	800	−1.473	−0.28	0.183	1.347×10^{-5}	3.689×10^{-9}	1.185×10^{-13}
450	800	−1.596	−0.123	0.145	2.482×10^{-5}	-1.218×10^{-9}	6.120×10^{-14}
550	800	−2.034	−1.326	0.106	1.407×10^{-4}	-1.066×10^{-8}	4.541×10^{-13}
600	800	−1.608	−0.232	1.220	8.941×10^{-4}	-5.302×10^{-8}	1.664×10^{-11}

Values of scaling exponents and coefficients of (42) versus compaction pressure and hardening temperature, a selection from [26].

Table 7. Somaloy 500.

Therefore, the considered binary relation is the strong inequality and corresponds to natural order presented in **Figures 15** and **16**. The most important question of this research is whether (45) is invariant with respect to scaling:

$$\frac{P'_{tot1}}{B'^{\beta 1}_{m1}} > \frac{P'_{tot2}}{B'^{\beta 2}_{m2}}. \tag{46}$$

Let $\lambda > 0$ be an arbitrary positive real number. Then, the scaling of (46) goes according to the following algorithm:

- Let us perform the scaling with respect to λ of all independent magnitudes and the dependent one:

$$f'_i = \lambda^{a_i} f_i; B'_{mi} = \lambda^{b_i} B_{mi}; P'_{tot} = \lambda^{c_i} P_{tot}, \tag{47}$$

  where $i = 1, 2 \ldots 4$ labels the considered characteristics.

- Substituting appropriate relations of (47) to (48), we derive:

$$\frac{P_{tot1}}{B^{\beta 1}_{m1}} \lambda^{c_1 - b_1 \beta_1} > \frac{P_{tot2}}{B^{\beta 2}_{m2}} \lambda^{c_2 - b_2 \beta_2}. \tag{48}$$

- Collecting all powers of λ on the left-hand side of (48) and taking into account (43) we derive that the resulting power has to be equal zero:

$$\lambda^{c_1 - b_1 \beta_1 - c_2 + b_2 \beta_2} = 1. \tag{49}$$

Therefore, (45) is invariant with respect to scaling. This binary relation has mathematical meaning and constitutes the total order in the set of characteristics.

Binary equivalence relations. The result derived in subsection **Scaling of binary relations** can be supplemented with the following binary equivalence relation. Let

$$X_{i,j=}\left(\frac{f_{i,j}}{B^{\alpha_i}_{mi,j}}, \frac{P_{toti,j}}{B^{\beta_i}_{mi,j}}\right) \tag{50}$$

be the jth point of the ith characteristic. Two points, j and k, are related if they belong to the same ith characteristic:

$$X_{i,j} \mathbf{R} X_{i,k}. \tag{51}$$

Theorem: **R** is equivalence relation. (The proof is trivial and can be done by checking out that the considered relation is reflexive, symmetric and transitive.) Therefore, **R** constitutes division of the positive-positive quarter of plane spanned by (50). The characteristics do not intersect each other except in the origin point which is excluded from the space. The result of this section implies that the power losses characteristics (27) and (42) are invariant with respect to scaling. Structure of derived here the set of all characteristics of which some examples are presented in **Figures 15** and **16** enable us to derive a formal pseudo-state equation of SMC. This equation constitutes a relation of the hardening temperature, the compaction pressure and a parameter characterizing the power losses characteristics corresponding to the values of these technological parameters. Finally, the pseudo-state equation will improve the algorithm for designing the best values of technological parameters.

Pseudo-equation of state for SMC. Let C is set of all possible power losses characteristics in considered SMC. Each characteristic is smooth curve in $[f/(B_m)^{\alpha}, Ptot/(B_m)^{\beta}]$ plane which corresponds to a point in $[T, p]$ plane. In order to derive the pseudo-state equation, we transform each power losses characteristic into a number V corresponding to (T, p) point. By this way, we obtain a function of two variables:

$$(T, p) \to V. \tag{52}$$

This function must satisfy the following condition. Let us concentrate our attention at the two following points:

$$\frac{f_1}{B_{m1}^{\alpha_1}} = \frac{f}{B_m^{\alpha}}; \frac{f_2}{B_{m2}^{\alpha_2}} = \frac{f}{B_m^{\alpha}}. \tag{53}$$

Let us consider the two characteristics $P_{tot1}/(B_{m1})^{\beta_1}$ and $P_{tot2}/(B_{m2})^{\beta_2}$ of the two samples composed in T_1, p_1 and T_2, p_2 temperatures and pressures, respectively, while the other technological parameters such as powder compositions and volume fraction are constant. Let us assume that for (53), the following relation holds:

$$\frac{P_{tot1}}{B_{m1}^{\beta 1}} > \frac{P_{tot2}}{B_{m2}^{\beta 2}} \tag{54}$$

It results from the derived structure of that (54) holds for each value of (53).Therefore, we have to assume the following condition of sought $V(T, p)$. If the relation (54) holds for given values of temperature and pressure T_1, p_1, T_2, p_2, then the following relation for $V(T, p)$ has to be satisfied:

$$V(T_1, p_1) > V(T_2, p_2). \tag{55}$$

Moreover, $V(T, p)$ has to indicate place of corresponding characteristic in the ordered set. The simplest choice satisfying these requirements is the following average:

$$V(T,p) = \frac{1}{\varphi_{\max} - \varphi_{\min}} \int_{\varphi_{min}}^{\varphi_{max}} \frac{P_{tot}\left(\frac{f}{B_m^{\alpha}}\right)}{B_m^{\beta}} d\left(\frac{f}{B_m^{\alpha}}\right), \tag{56}$$

The integration domain is common for all characteristics. We have selected the following common domain for the data presented in **Figures 15** and **16** $\varphi_{min} = 0$, $\varphi_{max} = 4000$ ($s^{-1}T^{-\alpha}$).

Using (42), we transform (56) to the working formula for the V we measure:

$$V(T,p) = \frac{1}{\varphi_{max} - \varphi_{min}} \int_{\varphi_{min}}^{\varphi_{max}} x\left(\Gamma_1 + x\left(\Gamma_2 + x(\Gamma_3 + x\Gamma_4)\right)\right) dx. \tag{57}$$

T	p	V
[K]	[MPa]	[W $kg^{-1}T^{-\beta}$]
723.15	800	40.60
773.15	900	43.75
773.15	700	47.25
673.15	800	50.30
773.15	600	57.12
823.15	800	81.50
773.15	500	89.28
742.15	764	492.3
753.15	780	509.2
804.15	764	528.5
711.15	764	547.0
873.15	800	720.0

Table 8. V measure versus hardening temperature and compaction pressure.

where $x = \frac{f}{B_m^{\alpha}}$ and Γ_i are coefficients dependent on T and p (see **Table 7**). The values of $V(T, p)$ are tabulated in **Table 8**. **Table 8** enables us to draw pseudo-isotherm. It is presented in **Figure 17**. However, in order to derive the complete pseudo-state equation, we must create a mathematical model. On the basis of **Figure 17**, we start from the classical gas state equation as an initial approximation:

http://dx.doi.org/10.5772/63285

$$\frac{p \cdot V}{k_B \cdot T} = 1. \tag{58}$$

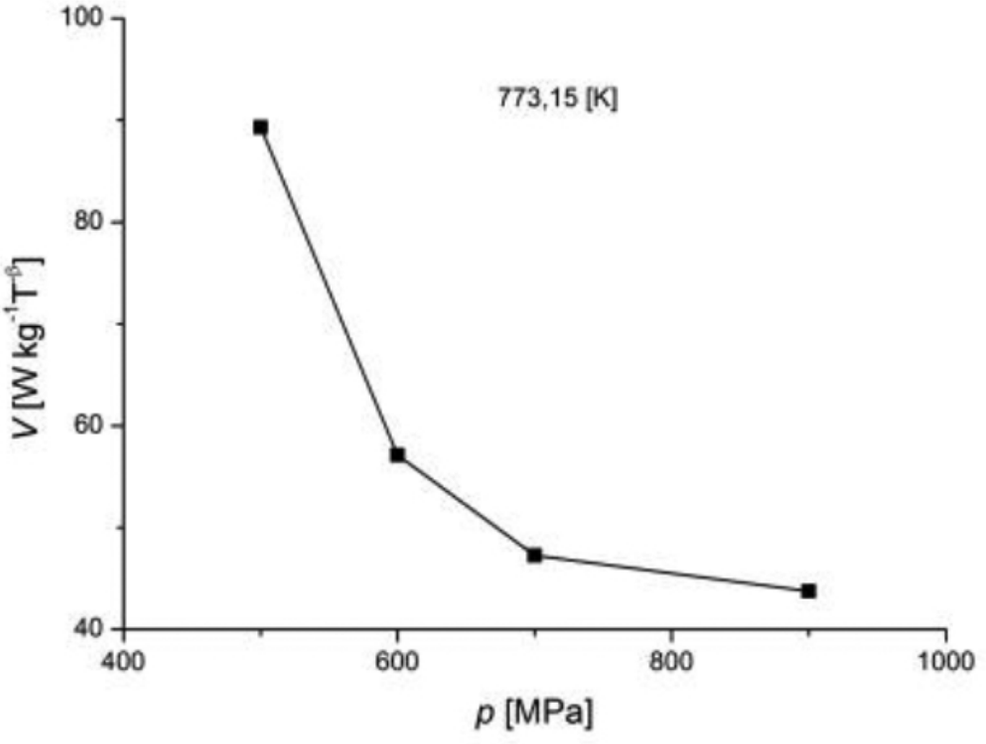

Figure 17. Pseudo-isotherm T = 500°C of the low-losses phase, according to data of **Table 8**. for Somaloy 500 [1].

where k_B is the pseudo-Boltzmann constant.

In order to extend (58) to a realistic equation, we apply again the scaling hypothesis (27):

$$V\left(\frac{T}{T_c}, \frac{p}{p_c}\right) = \left(\frac{p}{p_c}\right)^{\gamma} \Phi\left(\frac{\frac{T}{T_c}}{\left(\frac{p}{p_c}\right)^{\delta}}\right). \tag{59}$$

where Φ(•) is an arbitrary function to be determined. Parameters γ, δ and T_c, $p_c$are scaling exponents and scaling parameters, respectively, to be determined. For our conveniences, we introduce the following variables:

$$\tau = \left(\frac{T}{T_c}\right);\ \pi = \frac{p}{p_c}; X = \frac{\frac{T}{T_c}}{\left(\frac{p}{p_c}\right)^{\delta}} = \frac{\tau}{\pi^{\delta}}. \tag{60}$$

In order to extend (58) to a full-state equation, we apply the Padé approximant by analogy to virial expansion derived by [27]:

$$V(\tau,\pi) = \pi^{\gamma}\frac{G_0 + X\left(G_1 + X\left(G_2 + X\left(G_3 + XG_4\right)\right)\right)}{1 + X\left(D_1 + X\left(D_2 + X\left(D_3 + XD_4\right)\right)\right)}, \tag{61}$$

where G_0,…, G_4, D_1,… D_4 are coefficients of the Padé approximant. All parameters have to be determined from the data presented in **Table 8**.

Estimation of parameters for pseudo-equation of state. At the beginning, we have to notice that the data collected in **Table 8** reveal sudden change of V between two points: [773, 15; 500, 0] and [742, 15; 764, 0]. This suggests existence of a crossover between two phases: low-losses phase and high-losses phase. We take this effect into account and we divide the data of **Table 8** into two subsets corresponding to these two phases, respectively. Since the crossover consists in changing of characteristic exponents for the given universality class, it is necessary to perform estimations of the model parameters for each phase separately. Minimizations of χ^2 for both phases have been performed by using MICROSOFT EXCEL 2010, where

$$\chi^2 = \sum_{i=1}^{N}\left(V(\tau_i,\pi_i) - \pi_i^{\gamma}\frac{G_0 + X_i\left(G_1 + X_i\left(G_2 + X_i\left(G_3 + X_iG_4\right)\right)\right)}{1 + X_i\left(D_1 + X_i\left(D_2 + X_i\left(D_3 + X_iD_4\right)\right)\right)}\right)^2. \tag{62}$$

γ	δ	T_c	p_c	G_0	G_1	G_2
1.2812	0.1715	21.622	37.729	370315315	−47752251	1734952
G_3	G_4	D_1	D_2	D_3	D_4	–
−1.3764	−678.26	170.80	6243.8	386.96	−28.699	–

Values of pseudo-state equation's parameters and the Padé approximant's coefficients of (61)

Table 9. Somaloy 500, low-losses phase.

γ	δ	T_c	p_c	G_0	G_1	G_2
1.5550	0.1810	22.949	30.197	365210688	−47714207	1762773
G_3	G_4	D_1	D_2	D_3	D_4	–
−1.3763	−683.38	170.77	5739.9	387.81	−22.514	–

Values of pseudo-state equation's parameters and the Padé approximant's coefficients of (61)

Table 10. Somaloy 500, high-losses phase.

where $N = 7$ and $N = 5$ for the low-losses and high-losses phases, respectively. **Tables 9** and **10** present estimated values of the model parameters for the low-losses and high-losses phases, respectively.

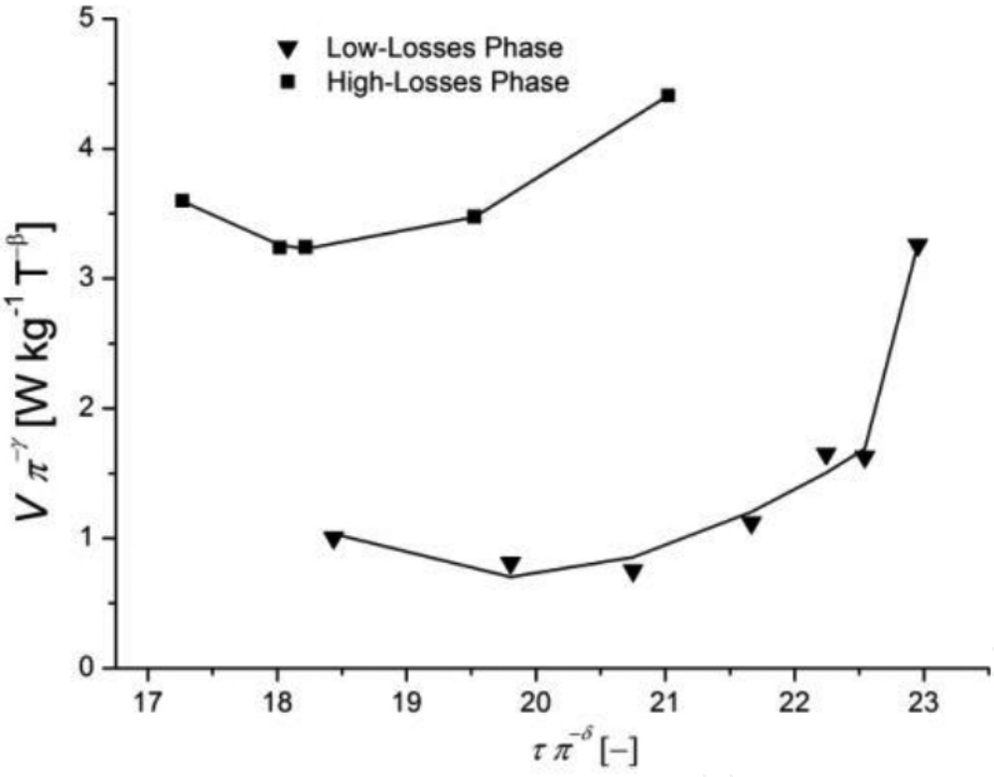

Figure 18. Phase diagram for Somaloy 500.

Optimization of technological parameters. Function $V(T, p)$ serves a power loss measure versus the hardening temperature and compaction pressure. In order to explain how to optimize the technological parameters with the pseudo-state Eq. (61), we plot the phase diagram of considered SMC **Figure 17**. Note that all losses' characteristics collapsed to a one curve for the each phase. Taking into account the low-losses phase, we determine the lowest losses at $\tau \cdot \pi^{-\delta} = 19, 75$ (see **Figure 18**). This gives the following continuous subspace of the optimal points:

$$\frac{\frac{T}{T_c}}{\left(\frac{p}{p_c}\right)^{\delta}} = 19,75. \tag{63}$$

Formula (63) represents the minimal iso-power loss curve. All points satisfying (63) are solutions of the optimization problem for technical parameters of SMC. By introducing the binary relations, we have revealed twofold. The power losses characteristics do not cross each other which makes the topology's set of these curves very useful and effectively that we can perform all calculations in the one-dimensional space spanned by the scaled frequency or here in the case of pseudo-state equation in the scaled temperature. For general knowledge concerning such a topology, we refer to the paper [28]. The obtained result is the continuous set of points satisfying (63). All solutions of these equations are equivalent for the optimization of the power losses. Therefore, the remaining degree of freedom can be used for optimizing the magnetic properties of the considered SMC.

6. Scaling conception of losses separation

In this section, we show how to expand losses into polynomial series. The distinction between different eddy current scales, that is a macroscale, covering the whole bulk material and a microscale covering the area of moving domain walls, introduced by Bertotti's theory, has led to the following relationship of the three terms:

$$P_{tot} = c_1 f B_m^{\beta} + c_2 \sigma f^2 B_m^2 + 8\sqrt{(\sigma G S V_0)} f^{1.5} B_m^{1.5}, \tag{64}$$

where σ is conductivity, G is the constant equal to 0.1356; S is sample cross section, whereas V_0 is a parameter dependent on flux density. In general case, (64) is not homogenous expression; therefore, this can describe the self-similarity property only for $\beta = 1$. However, the Bertotti interpretation of each term is correct

$$P_{tot} = P_{hys} + P_{clas} + P_{exc}. \tag{65}$$

where the presented in (65) components are hysteresis, classical and excess losses, respectively.

In this chapter, we have shown how the two-component formula for losses (28) can be transformed to dimensionless expression (30) and (31). This expression helps us to consider the data collapse. However, in the case of expansion of (27) over the square term, (31) does not apply.

Then, one can consider partial data collapses in the expansions up to necessary degree. Let us consider, for example, (42):

$$\frac{P_{tot}}{B_m^{\beta}} = \left(\Gamma_1 \cdot (f/B_m^{\alpha} + \cdot\Gamma_2 \cdot (f/B_m^{\alpha})^2 + \Gamma_3 \cdot (f/B_m^{\alpha})^3 + \Gamma_4 \cdot (f/B_m^{\alpha})^4\right),$$

Formula (42) is the fourth-degree polynomial of the (f/B_m^{α}) scaled frequency. Let us span all possible binomial subspaces:

$$\sum = \{S_{12}, S_{13}, S_{14}, S_{23}, S_{24}, S_{34}\},$$

where $S_{ij} = \left\{(f/(B_m^{\alpha}))^i, (f/(B_m^{\alpha}))^j\right\}$. To consider partial data collapse in S_{12}, we perform the following transformations:

$$P_{tot1,2} = \frac{\Gamma_2 P_{tot}}{\Gamma_1^2 B_m^{\beta}}, f_{1,2} = \frac{\Gamma_2 f}{\Gamma_1 B_m^{\alpha}}. \tag{66}$$

Substituting (66) to (42), we get

$$P_{tot\ 1,2}(f_{1,2}) = f_{1,2}(1 + f_{1,2}) + f_{1,2}^3 \frac{\Gamma_1}{\Gamma_2^2}(\Gamma_3 + f_{1,2} \frac{\Gamma_1 \Gamma_4}{\Gamma_2}). \tag{67}$$

Note that (67) is dimensionless full formula for the scaled loss. Moreover, expression $f_{12}(1 + f_{12})$ is sample independent. The linear and square terms describe the hysteresis and the classical losses, respectively. The cubic and the fourth-order terms correspond to the excess losses. Moreover, the square and linear terms describe the partial data collapse in S_{12} [29]. Using (67), one can compare losses data of different measurements projected on S_{12} subspace. The analogical equations for the S_{34} subspace read:

$$P_{tot\ 3,4} = \frac{\Gamma_4^3 P_{tot}}{\Gamma_3^4 B_m^{\beta}}, f_{3,4} = \frac{\Gamma_4 f}{\Gamma_3 B_m^{\alpha}}, \tag{68}$$

$$P_{tot\ 3,4}(f_{3,4}) = f_{3,4}^3(1 + f_{3,4}) + f_{3,4} \frac{\Gamma_4^2}{\Gamma_3^3}(\Gamma_1 + f_{3,4} \frac{\Gamma_2 \Gamma_3}{\Gamma_4}). \tag{69}$$

Sample	α	β	Γ_1	Γ_2	Γ_3	Γ_4
P1	−2.347	−1.407	2.25E-03	7.96E-06	−5.19E-09	1.76E-12
P2	−1.519	−0.375	2.53E-03	6.79E-06	−6.48E-09	2.78E-12
P4	−2.372	−1.295	1.80E-02	2.04E-05	7.68E-09	−1.37E-12
P7	−2.437	−1.401	2.28E-03	1.05E-05	3.08E-07	−8.38E-10

Table 11. Scaling exponents and expansion coefficients.

Applying (68) and (69), one can complete the data comparison by considering partial data collapse using $f_{3,4}^{3}(1+f_{3,4})$ polynomial which is also sample independent. In the case of expansion (42), the comparisons performed in S_{12}, S_{34} spaces are completed. To test the presented comparison formalism, we present the following measurement data: P1—amorphous alloy $Fe_{78}Si_{13}B_9$, P2—amorphous alloy $Co_{71.5}Fe_{2.5}Mn_2Mo_1Si_9B_{14}$, P4—crystalline material-oriented electrotechnical steel shits 3% Si-Fe and P7—iron-nickel-alloy 79%Ni-Fe. Processed measurement data in the form of scaling exponents and expansion coefficients are presented in **Table 11**:

Figures 19 and **20** present the completed partial collapses for the considered problem:

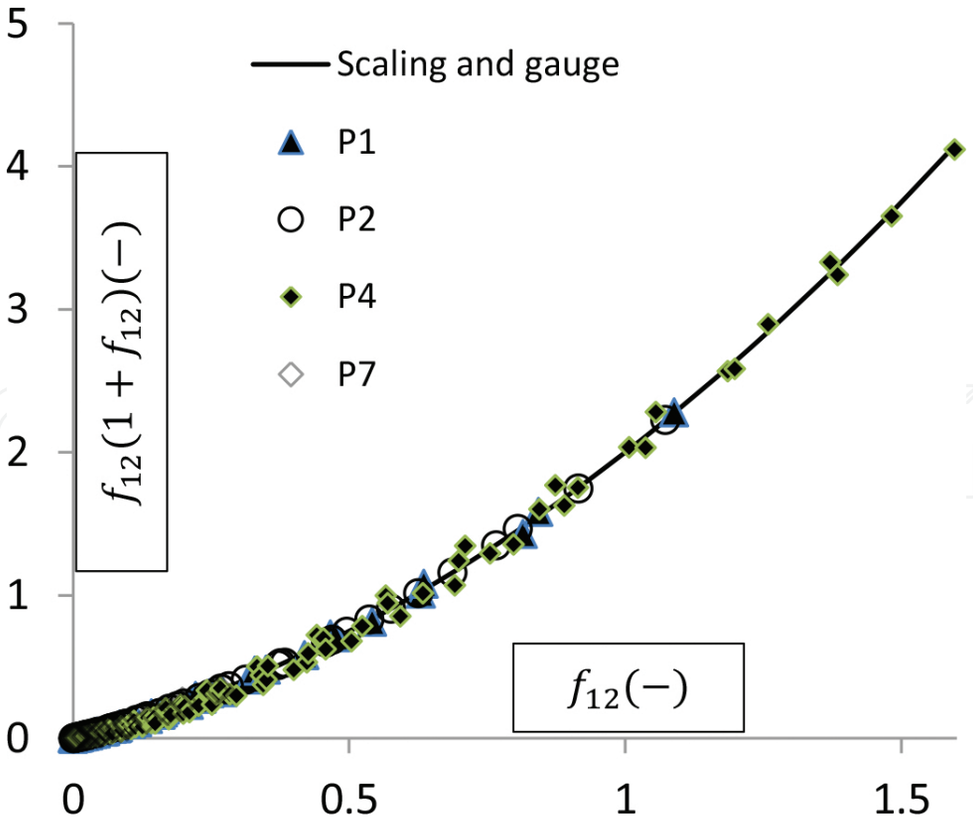

Figure 19. Partial data collapse in S_{12} space.

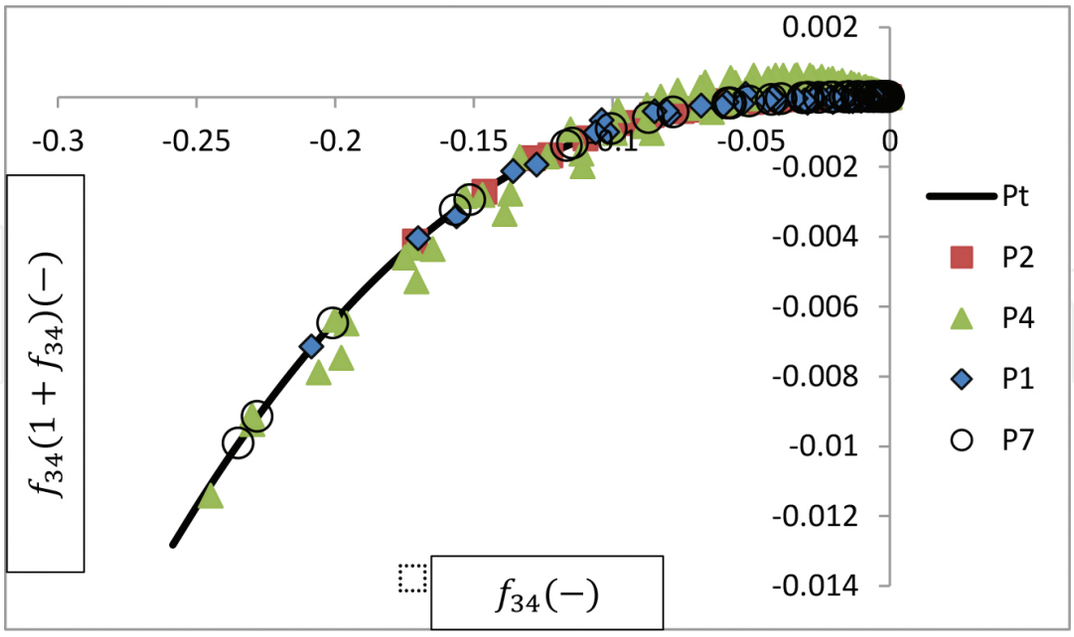

Figure 20. Partial data collapse in S_{34} space.

In order to make a numerical comparison of the measurement qualities taken from different samples, one can introduce analogically to (32) the measures of uncertainty for the both spaces S_{12} and S_{34}. The comparisons must be done and interpreted independently for S_{12} and S_{34}. Qualitative analysis on the basis of **Figures 19** and **20** shows that the uncertainty measure of S_{34} for the sample P_4 is significantly high.

7. Summary

We have presented many examples of the measurements of power losses in soft magnetic materials, including composites. Moreover, working conditions were determined by multidimensional parameter space: frequency, pick of induction, DC bias and temperature. On the basis of obtained results of experimental and theoretical considerations, we confirm that the total power loss in soft magnetic materials is self-similar. This is very important for practices, since the fundamental parameter used by technologists in the processes aimed at tailoring properties of magnetic materials as well as in design and work analysis of magnetic circuits is loss density. However, there is one important detail which has to be discussed at the end. In order to determine $F(\cdot)$ in (27), the Maclaurin expansion has been applied up to the second-order term. Note that each two-term formula can be reduced to dimensionless form (28). Therefore, one could conclude that the data collapse is trivial. However, this is not so because relevance of the data collapse depends on measurement data. If data transformed by (30) get place on (31), then these data satisfy the axioms of homogeneity, they are invariant with respect to scaling as well as they are self-similar. What to do if the two-term expansion (28) is not sufficient? Then, one should extend (28) up to sufficient polynomial order. For an example,

see (42). In general case, reduction of losses characteristic to dimensionless form is not possible. However, for comparison of different measurement data, it is possible always to perform transformation of data to dimensionless magnitudes partially in the two-dimensional subspaces (67), (69) and obtain full comparison by collecting the all independent comparisons in S_{ij} subspaces.

Author details

Krzysztof Z. Sokalski[1*], Barbara Ślusarek[2] and Jan Szczygłowski[1]

*Address all correspondence to: ksokalski76@gmail.com

1 Czestochowa University of Technology, Czestochowa, Poland

2 Tele and Radio Research Institute, Warszawa, Poland

References

[1] Barenblatt G.I. Scaling. Cambridge Texts in Applied Mathematics. Cambridge: Cambridge University Press; 2003. 52 p.

[2] Hamermesh M. Group Theory and Its Application to Physical Problems. London: Pergamon Press; 1962. 1–30 pp.

[3] Stanley H.E. Introduction to Phase Transitions and Critical Phenomena. Oxford: Clarendon Press; 1971. 78 p.

[4] Takaćs J. A phenomenological mathematical model of hysteresis. COMPEL: Int. J. Comput. Math. Electr. Electron. Eng. 2001;20:1014–1022. doi:10.1108/EUM0000000005771

[5] Sokalski K.Z. An approach to modeling and scaling of hysteresis in magnetic materials. Magnetization curve. Acta Phys. Pol. A. 2015;127:850–853. doi:10.12692/APhysPolA.127.850

[6] Preisach F. On the magnetization phenomenon. Z. Phys. 1935;94:277. doi:10.1007/BF01349418

[7] Mayergoyz I.D. Mathematical Models of Hysteresis. New York: Springer-Verlag; 1991

[8] Sokalski K.Z. Modeling and Scaling of Hysteresis in Magnetic Materials. Frequency, Pick of Induction and Temperature Dependence, arXiv:1510.06635v1 [physics.gen-ph]. doi:10.13140/RG.2.1.3909.44802015-10-19T17:34:48UTC

[9] Sokalski K.Z., Jankowski B., Ślusarek B. Binary relations between magnitudes of different dimensions used in material science optimization problems. Pseudo-state

equation of soft magnetic composites. Mater. Sci. Appl. 2014;5:1040–1047. doi:10.4236/msa.2014.514107

[10] Folders S. Fundamental Structures of Algebra and Discrete Mathematics. New York: John Wiley & SONS, Inc.; 1994.

[11] Bozorth R.M. Ferromagnetism. New York: IEEE Magnetic Society; 1993.

[12] Bertotti G. A general statistical approach to the problem of Eddy current losses. J. Magn. Magn. Mater. 1984;41:253–260. doi:10.101.6/0304-8853(84)90192-6

[13] Szczygłowski J., Kopciuszewski P., Wilczyński W., Roman A. Energy losses in Fe-based and Co-based amorphous materials. Mater. Sci. Eng. B 2000;75:13–16. doi:10.1016/S0921-5107(00)00376-7

[14] Sokalski K.Z. Integral and differential dependence between losses and hysteresis in magnetic materials. 2016 (submitted to Acta Physica Polonica a)

[15] Sokalski K., Szczygłowski J., Najgebauer M., Wilczyński W. Losses scaling in soft magnetic materials. COMPEL: Int. J. Comput. Math. Electr. Electron. Eng. 2007;26:640–649. doi:10.1108/03321640710751118

[16] Sokalski K., Szczygłowski J. Data collapse of energy loss in soft magnetic materials as a way for testing measurement set. Acta Phys. Pol. Ser. A 2010;117:497–499.

[17] Sievert J., Ahlers H., Birkfeld M., Cornut B., Fiorillo F., Hempel K.A, Kochmann T., Kedous-Lebouc A., Meydan T., Moses A., Rietto AM. European inter-comparison of measurements of rotational power loss in electrical sheet steel. J. Magn. Magn. Mater. 1996;160:115–118. doi:10.1016/0304-8853(96)00129-1

[18] Yuan W.J., Liu F.J., Pang S.J., Song Y.J., Zhang T. Core loss characteristics of Fe-based amorphous alloys. Intermetallic. 2009;17:278–280. doi:10.1016/j.intermet.2008.07.016

[19] Sokalski K., Szczygłowski J. Formula for energy loss in soft magnetic materials and scaling. Acta Phys. Pol. A 2009;115:920–924.

[20] Sokalski K., Szczygłowski J. Core losses under DC bias condition based on scaling. 2011. PLCRC/50002437/02/1725/2011 REPORT, ABB CRACOW.

[21] Van den Bossche A., Valchev V. Modeling ferrite core losses in power electronics. Int. Rev. Electr. Eng. 2006;1:14–22.

[22] Mühlethaler J., Biela J., Kolar J.W., Ecklebe A. Improved core-loss calculation for magnetic components employed in power electronic systems. IEEE Trans. Power Electron. 2012;27:964–973. doi:10.1109/TPEL.2011.2162252

[23] Nedler J.A., Mead R. A simplex method for a function minimization. Comput. J. 1965;7:308–313. doi:10.1093/comjnl/7.4.308

[24] Mühlethaler J., Biela J., Kolar J.W., Ecklebe A. Core losses under the DC bias condition based on Steinmetz parameters. IEEE Trans. Power Electron. 2012;27:953–963. doi: 10.1109/TPEL.2011.2160971

[25] Ruszczyk A., Sokalski K.Z. Unified model of temperature dependence of core losses in soft magnetic materials exposed to non-sinusoidal flux waveforms and DC bias condition. COMPEL: Int. J. Comput. Math. Electr. Electron. Eng. 2001;20:1014–1023. doi:10.1108/COMPEL-11-2013-0407

[26] Ślusarek B., Jankowski B., Sokalski K., Szczygłowski J. Characteristics of power loss in SMC a Kay for designing the best values of technological parameters. J. Alloys. Comp. 2013;581:699–704. doi:10.1016/j.jallcom.2013.07.084

[27] Ree F.H, Hoover W.G. Fifth and sixth virial coefficients for hard spheres and hard disks. J. Chem. Phys. 1964;40:939–950. doi:10.1063/1.1725286

[28] Egenhofer M.J. A formal definition of binary topological relationships. In: Proceedings of the Third International Conference on Foundations of Data Organization and Algorithms (FODO); Paris, France. Lecture Notes in Computer Science, 367, (Springer-Verlag, New York, June 1989) pp. 457–472.

[29] Sokalski K., Szczygłowski J., Wilczyński W. Scaling conception of energy loss' separation in soft magnetic materials. Int. J. Condens. Matter Adv. Mater. Supercond. Res. 2014;12(4):1–16. See also arXiv:1111.0939v1. doi:10.13140/2.1.2394.8489